Axonal TDP-43 Drives NMJ Disruption through Inhibition of Local Protein Synthesis

Topaz Altman
Tel Aviv University
Ariel Ionescu
Tel Aviv University
Amjad Ibraheem
Tel Aviv University
Dominik Priesmann
University of Cologne https://orcid.org/0000-0002-4898-0533
Tal Gradus-Pery
Tel-Aviv University
Luba Farberov
Tel-Aviv University
Gayster Alexandra
Sheba Medical Center
Natalia Shelestovich
Sheba Medical Center
Noam Shomron
Tel Aviv University
Amir Dori
Sheba Medical Center
Marcus Krueger
Uni Koeln
Eran Perlson (eranpe@tauex.tau.ac.il)
Tel Aviv University

Article

Keywords: Intra-muscular Nerves, Motor Neurons, Neuromuscular Junctions, Motor Neuron Axons, Nuclear-encoded Mitochondria Proteins

Posted Date: November 2nd, 2020

DOI: https://doi.org/10.21203/rs.3.rs-87662/v1

Axonal TDP-43 Drives NMJ Disruption through Inhibition of Local Protein Synthesis

Topaz Altman[1]*, Ariel Ionescu[1]*, Amjad Ibraheem[1], Dominik Priesmann[2], Tal Gradus-Pery[1], Luba Farberov[1], Gayster Alexandra[3], Natalia Shelestovich[3], Noam Shomron[1,5], Amir Dori[1,4], Marcus Krüger[2] and Eran Perlson[1,5]#

[1] Sackler Faculty of Medicine, Tel-Aviv University, Tel-Aviv, Israel.
[2] CECAD Research Center and Center for Molecular Medicine (CMMC), University of Cologne, 50931, Cologne, Germany
[3] Pathology Institute, Sheba Medical Center, Tel Hashomer, Ramat Gan, Israel
[4] Department of Neurology, Sheba Medical Center, Tel Hashomer, Ramat Gan, Israel
[5] Sagol School of Neuroscience, Tel-Aviv University, Tel-Aviv, Israel.

* These authors contributed equally to this work

#Corresponding author:
Eran Perlson, Ph.D., Dept. of Physiology and Pharmacology, Sackler Faculty of Medicine, Room 605, Sagol School of Neuroscience, Tel Aviv University, Ramat Aviv, Tel Aviv 69978, Israel. +972-3-6408743
E-mail: eranpe@tauex.tau.ac.il

Abstract

Mislocalization of the predominantly nuclear RNA/DNA binding protein, TDP-43, occurs in motor neurons of ~95% of ALS patients, but the contribution of axonal TDP-43 to this fatal neurodegenerative disease is unclear. Here, we find TDP-43 accumulation in the axons of intra-muscular nerves from ALS patients, and in motor neurons and neuromuscular junctions (NMJs) of a mouse model with TDP-43 mislocalization. This leads to the formation of G3BP1- and TDP-43- positive RNA-granules in motor neuron axons, and to inhibition of local protein synthesis in axons and NMJs. Specifically, the axonal and synaptic levels of nuclear-encoded mitochondria proteins are reduced. Clearance of axonal TDP-43 restored local translation of the nuclear-encoded mitochondrial proteins and rescued TDP-43-derived axonal and NMJ toxicity. These findings suggest that targeting TDP-43 axonal gain of function may mediate a therapeutic effect in ALS.

Introduction

Amyotrophic lateral sclerosis (ALS) is a fatal adult-onset neurological disease characterized by neuromuscular junction (NMJ) disruption and motor neuron degeneration[1,2]. An important pathological hallmark in ALS patients is the mislocalization of the primarily nuclear RNA and DNA binding protein, TAR DNA-binding protein 43 (TDP-43), to the cytoplasm of motor neurons[3–6]. TDP-43 is a member of the heterogeneous ribonucleoprotein binding protein (hnRNP) family, and have roles in transcription, RNA splicing, processing, and nucleocytoplasmic transport[4,7–9]. Additionally, mutations in TDP-43 were identified in a subset of ALS patients[10]. Cytoplasmic accumulation of TDP-43 has been implicated in ALS via several pathways[11], but the mechanism sensitizing motor neurons and the NMJ to TDP-43 proteinopathy remains unclear.

One key event which develops due to TDP-43 mislocalization is the formation of phase separated cytoplasmic condensates that are associated with alterations in RNA localization and translation[12–14]. In addition, ALS-associated mutations in TDP-43 can directly interfere with mRNA transport[15,16]. This process is associated with development of pathological RNP condensates[16], which were shown to deregulate mRNA localization and translation[17,18].

The formation of RNP granules[18] and mRNA transport[19] affect localized protein synthesis, an important regulator of axonal and synaptic health in different neuronal subtypes[20–23]. Several recent studies demonstrated alterations of protein synthesis in ALS models[13,24,25]. However, most of those observations were made in non-neuronal cells or within the neuronal cell body, not in the NMJ. Given that the NMJ and motor neuron axons are the first compartments to fail in ALS[26,27], the consequences of TDP-43 mislocalization in these compartments are key to understanding disease pathology.

To study the effect of TDP-43 mislocalization on the NMJ in a precise and controlled environment, we used a neuromuscular co-culture setup in microfluidic chambers (MFCs) that we recently developed[28–32]. This platform can model several pathological features of ALS, such as axon degeneration, NMJ dysfunction and MN death[29,33–35]. The fluidic separation between the motor neuron cell-body and axon allows the formation of functional NMJs exclusively at the distal compartment[29,31–36]. Utilizing this system, it is possible to study and track spatiotemporal events such as localized protein synthesis at the subcellular level.

Here, we describe a novel, toxic gain-of-function of TDP-43 accumulation in axons and NMJs, which impacts synaptic local protein synthesis and provokes neurodegeneration. By employing muscle biopsies from ALS patients, we demonstrate TDP-43 pathology in distal motor neuron axons. This mislocalization leads to formation of axonal RNP-complexes that interfere with local synthesis in axons and NMJs. Furthermore, the local synthesis of nuclear-encoded mitochondrial proteins is specifically inhibited, consequently promoting NMJ

dysfunction. Most strikingly, the clearance of TDP-43 from axons reverses the pathological events, shedding light on the possibility for MN recovery in ALS.

Results

TDP-43 Accumulates in ALS Patients Intra-Muscular Nerves and in Motor Axons of TDPΔNLS Mice

TDP-43 mislocalizes to the cytoplasm in ALS patient spinal cord MNs, where it is often observed as insoluble aggregate-like structures[3,4]. However, it is not clear how this process can cause distal degeneration of axons and the NMJ up to one meter away from the cell body. To determine whether TDP-43 mis-localization also occurs in distal axons, we immuno-stained muscle biopsies from ALS patients and non-ALS controls and compared the abundance of TDP-43 in their intra-muscular nerves (Fig.1A). Axonal levels of both TDP-43 and its phosphorylated form[3] significantly increased by ~1.5-fold in ALS patients (Fig.1B-E). Thus, TDP-43 nuclear-to-cytoplasmic mislocalization propagates to distal MN axons in ALS patients. To study the role of TDP-43 mislocalization in ALS pathology, we utilized inducible transgenic mice expressing the human TDP-43 lacking the nuclear-localization-signal (ΔNLS) through the doxycycline (dox) TET-off system. This TDPΔNLS mouse model recapitulates ALS-like MN disease pathologies[37–39], including NMJ disruption, in a mechanism that is still not fully understood. To allow close monitoring of MNs in the diseased mice, TDPΔNLS mice were cross-bred to Choline-Acetyltransferase (ChAT)^{cre}-tdTomato^{lox} mice (hereafter ChAT^{tdTomato}). Retraction of dox from adult animals, as well as in primary motor neuron culture, resulted in TDP-43 cytoplasmic mislocalization in MNs (Supp. Fig. 1A-B). To determine whether TDP-43 mislocalization is accompanied by its propagation into axons, we developed a novel radial MFC (Fig. 1F, upper panel), which allows collection of large quantities of pure axonal protein and RNA (Sup. Fig. 1C-D). We found a 2-fold increase in axonal TDP-43 levels upon dox-retraction in MNs (Fig.1F lower panel, and 1G; Sup. Fig. 1E). A similar effect was seen in TDPΔNLS mice sciatic nerves (SN; Fig.1H-J) and NMJs (Fig.1K). Thus, TDP-43 in TDPΔNLS mice is mislocalized to remote axons and synapses, far from MN cell-bodies, similar to our observations from ALS patients muscle biopsies.

Increased Levels of Axonal TDP-43 Lead to the Formation of G3BP1 positive RNP Condensates.

Upon its perinuclear mislocalization in ALS MNs, TDP-43 can form insoluble aggregate-like RNP structures[12–14]. To determine whether this occurs in axons, we grew primary MN cultures in the MFC system, and tested TDP-43 colocalization with axonal RNP component, Ras GTPase-activating protein-binding protein 1 (G3BP1)[17,18]. Upon dox retraction, TDP-43 extensively colocalized with G3BP1 in TDPΔNLS MN axons (Fig.2A-C). This likely occurs both

due to the observed increased TDP-43 and G3BP1 levels (Fig. 2D-E), and increased colocalization (Sup. Fig. 2A-B). Notably, by labeling RNAs with SYTO RNA select dye[15], we found that RNA, a critical component of cytoplasmic RNP aggregates, was enriched in the axonal TDP-43-G3BP1 complexes (Fig.2F-H). Thus, axonal accumulation of TDP-43 leads to the appearance of G3BP1 positive RNP structures in axons.

TDP-43 Axonal Accumulation Leads to a Profound Reduction in MN Axonal and NMJ Local Protein Synthesis.

Formation of G3BP1 positive RNP granules is strongly associated with repression of RNA translation[18] and with altered mRNA transport[17], leading to reduced protein synthesis[18]. Axonal and synaptic protein synthesis are vital for the proper neuronal function and facilitation of synaptic transmission[22,40]. Although local protein synthesis has not yet been described in the MN synapse, the NMJ, being the largest and most distant of all synapses, most likely relies on local synthesis for its maintenance. We therefore sought to determine whether TDP-43 axonal accumulation, and the subsequent RNPs formation, impair local synthesis in MN axons and NMJs. To test this, we cultured primary MNs from TDPΔNLS in MFC, and applied O-Propargyl-Puromycin (OPP) to the axonal compartment to exclusively label newly synthesized proteins in axons. We found a substantial decrease in density of the OPP puncta in TDPΔNLS (Fig. 3A-B) demonstrating reduced local synthesis upon cytoplasmic accumulation of TDP-43 in axons. The level of the local synthesis impairment we observed in TDPΔNLS was similar to that seen by inducing RNP-granule formation in axons with compartmental application of sodium-arsenite ($NaAsO_2$), or by direct pharmacological inhibition of local synthesis using Anisomycin and Cycloheximide (Sup. Fig. 3A-I). Next, we aimed to evaluate local synthesis also in the most distant point of the MN axon, the NMJ. To that end, we performed co-cultures of TDPΔNLS MNs with healthy-puromycin resistant muscles (Sup. Fig. 3J-L) and quantified the OPP puncta density within *in-vitro* NMJs. We identified robust NMJ protein synthesis in the control co-culture system. However, the majority of TDPΔNLS NMJs were devoid of OPP signal, or had very low OPP density, indicating impaired local synthesis (Fig. 3C-D). Furthermore, we observed a similar decrease in OPP density in NMJs following $NaAsO_2$ application only in the NMJ side of the compartmental MFC platform (Sup. Fig. 4M-N). Following these findings, we examined the extent of protein synthesis and its interference in adult TDPΔNLS mice. To that end, we labeled SNs and tibialis anterior (TA) muscles with OPP immediately after their dissection (Sup. Fig. 4A; see methods)[20]. Quantification of the OPP signal intensity within ChAT positive axons revealed a ~2-fold reduction in the amount of newly synthesized proteins in the TDPΔNLS SN compared to their littermates (LM; Fig. 3E-F, Sup. Fig. 4B). Next, we quantified the OPP signals that co-localized with ChAT in the NMJ pre-synapse (Sup. Movie. 1) and identified a significant reduction in protein synthesis in NMJs

from TDPΔNLS mice (Fig. 3G-H). Taken together, our *in-vitro* and *in-vivo* evidence demonstrate that TDP-43 axonal mislocalization disrupts axonal and presynaptic local synthesis at the NMJ.

TDP-43 Axonal Accumulation Results in Reduced Levels of Nuclear-Encoded Mitochondrial Proteins and Decreases Mitochondria-Associated Local Synthesis

To determine which proteins are primarily affected by TDP-43 accumulation and local synthesis reduction in axons, we performed proteome analysis of SN axoplasm samples from TDPΔNLS and LM control mice (Fig 4A). This revealed a global reduction in nuclear-encoded mitochondrial proteins (Mitocarta 2.0[41]), including respiratory chain complex proteins (Fig 4A-C, Sup. Table 1), implying that they are directly influenced by TDP-43 axonal accumulation and local synthesis inhibition. Additionally, the TDPΔNLS axoplasm was enriched with proteins from the "ribonucleoprotein complexes" family, including also TDP-43, thus reinforcing our observations regarding formation of RNP condensates in axons (Fig. 4C).

mRNAs of nuclear-encoded mitochondrial proteins are among the most abundant mRNAs in MN axons[42,43], therefore it is likely that the TDP-43-mediated reduction in local translation will primarily affect mitochondrial proteins. To determine whether the reduction in mitochondrial proteins occurs at the transcriptional or translational level, we performed RT-qPCR analysis on SN axoplasm and quantified the mRNA levels of three nuclear-encoded mitochondrial proteins: ATP5A1, Cox4i1, and Ndufa4, which were downregulated in TDPΔNLS axons (Protein Log_2FC over LM= -1.83; -1.21; -4.17 respectively). Conversely, we demonstrated that the relative axoplasmic mRNA levels of those proteins were unchanged and even moderately increased in TDPΔNLS samples (Fig 4D), implying that TDP-43 accumulation impairs the local translation of these mRNAs.

Localized translation in axons of some nuclear encoded mitochondrial proteins was recently shown to occur in proximity to the mitochondria[21]. To understand the relationship between TDP-43 accumulation and mitochondria-related local synthesis, we tested the extent of co-localization between mitochondria and OPP-labeled newly synthesized proteins in control versus TDPΔNLS axons. This analysis detected a profound reduction in the co-localization of mitochondria with OPP in TDPΔNLS axons (Fig. 4E-F). Next, we determined whether mitochondrial activity is directly dependent on local translation by measuring mitochondria membrane potential using TMRE dye (an indicator for mitochondria function) after axonal application of the protein synthesis inhibitor anisomycin, as well as following formation of RNP granules via $NaAsO_2$ treatment (Fig 4G). Inhibition of protein synthesis using both methods reduced axonal mitochondria membrane potential (Fig 4H). Thus, interfering with axonal local synthesis alters the function of axonal mitochondria.

Hence, we sought to identify whether the lack of mitochondria-related local synthesis due to TDP-43 axonal mislocalization also affects the function of axonal mitochondria. To this end, MN axonal mitochondria were challenged with a transient 4h protein synthesis inhibition using anisomycin, followed by a 24h recovery period. While TDPΔNLS axonal mitochondria failed to recover their initial TMRE signal, the membrane potential of mitochondria in control axons was recovered (Fig. 4I-J). Taken together, this suggests that mitochondrial proteins are especially vulnerable to the local synthesis inhibition mediated by TDP-43 axonal accumulation.

Mitochondria Activity and Local Protein Synthesis are Vital for NMJ Function and Their Inhibition Leads to Neurodegeneration

Thus far, our observations demonstrated that mislocalized TDP-43 forms RNP condensates along MN axons that interfere with protein synthesis events, specifically those of mitochondrial proteins. However, the functional outcome of this abnormal process is unclear. To this end, we first tested whether NMJ activity is dependent on general mitochondrial health using mitochondrial-targeted Killer-Red fusion protein (MKR)[40]. MKR was introduced into MNs in co-culture via lentiviral infection prior to muscle culturing. Upon NMJ formation, we damaged synaptic mitochondria by exclusively irradiating pre-synaptic MKR-expressing mitochondria (Fig. 5A-B). Live imaging of calcium transients in the post-synaptic muscle displayed a marked decrease in muscle activity following MKR irradiation (Fig. 5C-D, Sup. Movies 2-3). This suggests that pre-synaptic mitochondria are necessary to maintain NMJ activity.

Next, we inhibited local synthesis in pre-synaptic axons to determine if local synthesis has a similar contribution to NMJ function. To this end, we generated co-cultures of motor neurons with puromycin-resistant muscles (Sup. Fig.4G-I) and applied puromycin exclusively to the NMJ compartment of the MFC. Imaging calcium transients in post-synaptic muscles revealed a ~3.2-fold decrease in the number of active muscles following axonal and synaptic local synthesis inhibition (Fig.5E-H and Sup. Movies 4-5). Notably, we also observed decreased pairing between neuronal firing and muscle response (Fig.5G). These results indicate that local synthesis is fundamental to maintain active NMJs.

Finally, having identified that both mitochondria and local synthesis are essential for the NMJ, we aimed to determine if MN axons exhibit neurodegeneration in response to local synthesis inhibition. An evaluation of axon health over time revealed extensive degeneration 24-hour exposure to local synthesis inhibition (Sup. Fig. 5). Importantly, TDPΔNLS axons had a significantly increased sensitivity to local synthesis inhibition, displaying ~20% more degeneration compared to control axons (Fig. 5I-K) after 24-hours. Altogether, both mitochondrial integrity and the local synthesis that supports it play crucial roles in maintaining

axonal integrity. These processes are disrupted following TDP-43 mislocalization, which could eventually lead to NMJ dysfunction and neurodegeneration.

Restoring TDP-43 Localization Recovers Local Translation of Nuclear-encoded Mitochondrial Proteins and Enables NMJ Reinnervation.

Mislocalization of TDP-43 is a pathological hallmark in the majority of ALS cases, and mutations in TDP-43 cause familial ALS, indicating a converging mechanistic role of TDP-43 dysfunction in ALS pathogenesis[3–5,10]. We have shown here that TDP-43 propagates also to ALS patient axons (Fig.1). To study the effect of axonal TDP-43 clearance, similar to what was previously observed in MNs cell bodies[39], we investigated the ability of TDP∆NLS mice to recover after ceasing the expression of hTDP-43∆NLS and allowing endogenous TDP-43 to redistribute to its normal localization. We employed a recovery paradigm in which doxycycline was reintroduced into the diet of TDP∆NLS mice after initial deprivation (same was done for in vitro in primary MNs). After re-introducing doxycycline, we observed a decrease in the levels of hTDP-43 in SN axoplasm that was accompanied by a significant decrease in total TDP-43 levels (Fig. 6A). Interestingly, while TDP-43 levels in the SN and GC were substantially decreased in the recovered mice, TDP-43 levels in the spinal cord were more persistent (Sup. Fig. 6A), as also indicated by only partial recovery of TDP-43 to nuclei in spinal motor neurons (Sup.Fig. 6B-C). To further demonstrate the clearance of TDP-43 from MN axons and NMJs, we performed immunolabeling against tTDP-43 in SN sections and GC muscles. We observed a marked decrease of TDP-43 both in MN axons (Fig. 6B-C), and NMJs (Fig. 6D-E). Thus, TDP-43 condensates can be cleared from axons and NMJs.

To determine whether the clearance of TDP-43 axonal accumulation also releases the inhibitions on axonal and pre-synaptic local synthesis, we performed OPP labeling on MNs following a similar recovery paradigm. Strikingly, quantification of the OPP signal in the pre-synaptic side of NMJs revealed that MN protein synthesis returns to full capacity, both *in-vitro* (Fig. 6F-G) and *in-vivo* (Fig. 6H-I, Sup. Fig. 7A-B).

Next, given the sciatic proteome analysis, we analyzed whether TDP-43 mislocalization controls the local translation of nuclear-encoded mitochondrial genes in NMJs. First, by co-labeling NMJs in EDL muscles with OPP, and against the mitochondrial proteins Cox4i and ATP5A1, we showed that both proteins colocalize with OPP signals in NMJs, implicating that these undergo local translation (Fig. 6J-K, Sup. Fig. 7C-D). Importantly, quantification of the pre-synaptic occupancy of Cox4i or ATP5A1 signals (Sup. Movies 6) validated that they are deficient in NMJs of TDP∆NLS mice, and that clearance of TDP-43 restored their proper localization (Fig. 6L, Sup. Fig. 7E). Testing for the extent of colocalization between either Cox4i or ATP5A1 with pre-synaptic OPP indicated that their depletion in NMJs is dominated

by reduction in their local synthesis, which was also restored upon TDP-43 clearance (Fig. 6M, Sup. Fig. 7F).

Finally, to understand the functional impact of TDP-43 mislocalization on NMJ degeneration, and whether it could be reverted by applying the recovery paradigm, we measured the innervation rate in co-cultures of TDP∆NLS MNs and healthy muscles. This demonstrated that mislocalized TDP-43 facilitates NMJ dysfunction and disruption in co-cultures (Fig. 6N-O). Importantly, aside of axonal regeneration and NMJ reinnervation, TDP-43 clearance enabled functional recovery of NMJs as measured by the percent of innervated muscles that contract (Fig. 6P). Accordingly, recovered mice also demonstrated NMJ reinnervation (Fig. 6Q-R, Sup. Fig. 8A-C), and regained their weight, further supporting our findings (Sup. Fig. 8D).

Altogether, we show that the pathological mislocalization and accumulation of TDP-43 in MN axons disrupts axonal and synaptic local synthesis. This leads to altered mitochondrial protein turnover in axons and the NMJ, and eventually sensitizes the entire synapse to degeneration (Fig.7), a process which is reversible upon TDP-43 clearance.

Discussion

TDP-43 cytoplasmic mislocalization is a pathological hallmark of ALS, in both sporadic and familial cases[3–5]. Previous research on TDP-43 focused on the outcomes of cytoplasmic mislocalization in MN cell bodies[11,14]. Nonetheless, TDP-43 is regularly found in axons[44], where it serves a role in shuttling and localization of mRNAs[15]. Recent reports also revealed that TDP-43 is important for proper axonal local synthesis[45,46]. Here, we demonstrate that ALS patients display an increase in TDP-43 levels in intramuscular nerves, suggesting a forward propagation of TDP-43 to distal axons. We validate this process using an inducible model that mimics the cytoplasmic mislocalization of TDP-43. We then show that TDP-43 axonal accumulation elicits the formation of RNA and G3BP1 containing RNP granules in MN axons that consequently interfere with axonal and pre-synaptic local synthesis. This leads to depletion of nuclear-encoded mitochondrial genes. As we show, mitochondria related local synthesis is essential to maintain the axon and the NMJ, and interference with it leads to neurodegeneration (Fig. 7). Finally, we demonstrate that inhibition of local synthesis is reversible, thus providing novel findings regarding the mechanisms by which MN can cope with temporary insult to their local synthesis capacities and to mitochondrial alterations.

The concept of local synthesis in neuronal processes has mainly been studied in regenerative contexts[18,20,23], but recent data also suggests it is critical for understanding neurodegenerative disease mechanisms[21,24]. Our findings highlight how increased abundance of TDP-43, an RNA-binding protein hypothesized to play an important role in local synthesis, can become harmful when mobilized extensively into axons. This is associated with TDP-43 induced

formation of phase separated cytoplasmic RNP accumulations[12,14,47]. Recently, G3BP1 positive RNP granules were shown to inhibit translation[18]. We show that translation inhibition is strongly implicated upon TDP-43 axonal accumulation, which is associated with G3BP1 RNP colocalization (Fig. 2). Future work will be needed to further analyze the mechanisms through which local synthesis is regulated by formation of axonal RNP condensates.

A fundamental finding in this research is that local translation in NMJs is performed to a much greater extent than in axons (Fig. 3B vs. 3D). As NMJs are enriched with mitochondria[31,48,49], and due to mitochondrial dependency on local synthesis[21,50] (Fig 4G-H), the enhanced local synthesis in NMJs can be attributed to its mitochondrial density. This suggests that the high polarization of MNs leads to higher dependency on local synthesis of mitochondrial proteins. As we show, the NMJ relies on mitochondria activity (Fig. 5A-D)[31] and on local synthesis (Fig. 5E-G). Therefore, interference of synaptic local synthesis might initiate local energy deficiency that ultimately leads to NMJ degeneration. Taken together, these may supply a partial explanation for how TDP-43-mediated reduction in local synthesis specifically sensitizes the NMJs to rapid degeneration, and even further, why NMJ degeneration is an early pathology in ALS[26,51]. Further research will be needed to reveal the sequence of events, focusing on the initiation of mitochondrial toxicity in the NMJ.

Finally, we found that the TDP-43 cytoplasmic-related pathology could be reversed by ceasing TDP-43ΔNLS expression, leading to reduction in axonal TDP-43 and clearance of synaptic aggregates. Overall, recovered mice presented reinnervation of NMJs and regained their weight. This is a pivotal finding since in most ALS patients TDP-43 is not mutated, and yet it still mis-localizes to the cytoplasm and forms aggregates. Hence, regulating axonal levels of TDP-43 might reverse the disease outcome for a considerable number of patients, and become an important target for future drug development.

Online Material and Methods

Transgenic Mice

NEFH-tTA line 8 (Jax Stock No: 025397) and B6;C3-Tg(tetO-TARDBP*)4Vle/J (Jax Stock No: 014650) were obtained from Jackson Laboratories and cross-bred to create NEFH-hTDP-43ΔNLS (TDP43ΔNLS) mice line. Those mice were constitutively fed with doxycycline containing diet (200 mg/kg Dox Diet #3888, Bio-Serv) as was done previously[37–39]. $ChAT^{cre}$-$tdTomato^{lox}$ - hTDP-43ΔNLS was obtained by crossing the hTDP-43ΔNLS with $ChAT^{cre}$ and $tdTomato^{lox}$ mice, . (Jax stock no. 006410 and 007908, respectively).

After Dox retraction, all hTDP-43ΔNLS mice were weighted weekly to track disease progression.

HB9-GFP (Jax stock no. 005029) mice were originally obtained from Jackson Laboratories. The colony was maintained by breeding with ICR mice (Institute of Animal Science, Harlan). All animal experiments were approved and supervised by the Animal Ethics Committee of Tel-Aviv University.

Human muscle biopsy for intra-muscular nerve staining

Intra-muscular nerve staining was performed on muscle biopsies from 3 ALS patients and 5 non-ALS patients. All clinical and muscle biopsy materials used in this study were obtained with written informed consent during 2016-2020 for diagnostic purposes followed by research application, approved by the institutional review board. Deltoid, quadriceps or gastrocnemius skeletal muscle samples were excised via open biopsies and pathological analysis was performed at the neuromuscular pathology laboratory at Sheba Medical Center, Ramat-Gan, Israel. All 3 ALS patients were diagnosed with clinically definite or probable ALS according to El Escorial criteria[52]. Control muscles included a variation of findings, which were consistent with a diagnosis of normal muscle, severe, chronic ongoing denervation and reinnervation due to spinal stenosis, necrotic autoimmune myopathy, type 2 fiber atrophy due to disuse and overlap myositis syndrome.

Frozen muscle biopsies were than cryo-sectioned to 10µm thick slices, mounted onto slides and air dried for 30 minutes in room temperature (RT). Sections were than washed in PBS, fixed in 4% PFA for 20 min, and permeabilized with 0.1% Triton, and blocked with 5% goat serum (Jackson Laboratories) and 1 mg/mL BSA (Amresco). Sections were than incubated ON with appropriate antibodies overnight at 4°C in blocking solution [rabbit anti TDP43 or rabbit anti phospho TDP-43 (both 1:1,000, Proteintech), Chicken anti NFH (Abcam, 1:1,000). Sections were washed again and incubated for 2 hours with secondary antibodies (1:1,000, Jackson Laboratories and ThermoFisher), washed and mounted with ProLong Gold (Life Technologies).

Microfluidic chamber preparation

Our MFCs design was recently published[53]. Briefly, PDMS (Dow Corning) was casted into custom-made epoxy replica molds, left to cure overnight (ON) at 70^{o}C, punched (6mm / 7mm punches), cleaned and positioned in 35mm or 50mm glass plates (WPI): All experiments were done in 6mm-well small MFCs, except for experiments in Figure 2, where 7mm-wells MFC were punched for spinal cord explant culture[53].

Radial PDMS molds (Fig. 1G-J) were designed and fabricated with SU-8 photoresist protocol[54] in the Tel-Aviv University Nano and Micro Fabrication Center. as described in the following table:

Elements	Dimensions
Inner well diameter	7.5 mm
Inner well punch diameter	7 mm
Inner channel height	140 µm
Inner channel width	250 µm
Outer channel diameter	13 mm
Outer compartment punch diameter	9 mm
Outer channel width	200 µm
Outer channel height	140µm
Microgroove width	10µm
Microgroove length	300µm
Microgroove height	5µm
Microgroove spacing	15µm
Pod dimensions	450µm x 300µm

PDMS mold was pre-treated with Chlorotrimethylsilane (Sigma) prior to PDMS casting. PDMS casting was done in a similar manner as for regular MFC. Radial MFCs were then punched twice to form MFC rings. Inner well was punched with 7mm biopsy punch, and outer well was punched with 9mm punch. Cleaning procedure done in a similar manner as for regular MFC. Radial MFC rings were adhered to sterile 13mm coverslips (Cat no.) inside 24-well plates.

MN culture and MN – myocyte co-culture

E12.5 old embryos ventral spinal cord were dissected in HBSS prior to dissociation. For TDP∆NLS cultures, genotype of each embryo was determined at this phase by PCR. Meanwhile, spinal cords were kept in 37°C 5% CO_2 with Leibovitz L-15 medium (Biological industries) supplemented with 5% Fetal Calf serum and 1% Penicillin/Streptomycin (P/S-Biological Industries). Spinal cord explants were cut transversely to small pieces and plated in MFC proximal compartment in Neurobasal (Gibco), 2% B27 (Thermo Fisher), 1% Glutamax (Gibco),1% P/S, 25 ng/mL BDNF (Alomone labs).

Dissociated MN cultures were obtained by further, trypsinization and trituration of explants. Supernatant was collected and centrifuged through BSA (Sigma) cushion. The pellet was then resuspended and centrifuged through and Optiprep (Sigma) gradient (containing 10.4% Optiprep, 10mM Tricine, 4%w/v glucose). MN-enriched fraction was collected from the interphase, resuspended and plated in the proximal MFC compartment at a concentration of 150,000 MN per regular MFC, 250,000 per radial MFC. MNs were maintained in complete

neurobasal (CNB) medium containing Neurobasal, 4% B27, 2% horse serum (Biological Industries), 1% Glutamax, 1% P/S, 25μM Beta-Mercapto ethanol, 25 ng/mL BDNF, 1ng/mL GDNF (Alomone) and 0.5ng/mL CNTF (Alomone). Glial cell proliferation was restricted by addition of 1μM Cytosine Arabinoside (ARA-C; Sigma) to culture medium in 1-3DIV. At 3DIV BDNF concentration in proximal compartment was reduced (1ng/mL), while medium in distal compartment was enriched with GDNF and BDNF (25ng/mL) to direct axonal growth.

Myocyte culture was performed as previously described[32,36]. Briefly, GC muscles from a P60 adult C57BL/6J mouse were extracted into DMEM with 2.5% P/S/N (Biological Industries) with 2 mg/mL collagenase-I (Sigma) for 3 hours, then dissociated and incubated with BioAmf 2.0 (BA; Biological Industries) in Matrigel (BD Corning) coated plates for 3 days. Myoblasts were purified by performing pre-plating for 3 consecutive days, and then plated at a density of 75,000 in small MFC, and 150,000 for large MFC (for SC explant experiments).

Muscles in co-culture were kept in BA medium for 7 days. To aid NMJ formation, media in all compartments was then replaced to poor neurobasal (PNB) medium, which contained only 1% P/S and 1% Glutamax. Doxycycline was applied to TDP-43ΔNLS cultures only at the proximal MN compartment, in a concentration of 0.1μg/mL, immediately after plating and throughout the entire experimental timeline.

Protein Extraction

Spinal cord and GC muscles were extracted from adult mice and homogenized in ice-cold PBS lysis buffer containing 1% Triton and protease inhibitors (Roche). SN axoplasm was obtained from both SNs from every mouse. SNs were sectioned and axoplasm was extracted into 100μL PBS and protease inhibitors by gentle pressing the sections.

Extraction of axonal and somatic proteins from radial MFCs was performed as follows: Axons were extracted by first filling the inner well with high volume of PBS and applying 40μL of RIPA lysis buffer (1% Triton, 0.1% SDS, 25 mM Tris-HCl (pH 8.0), 150 mM NaCl) to the outer compartment for 1 minute. We used the same 40μL to collect the axon lysate from two additional wells – in total, 3 wells per sample. Protein extraction from the inner (soma) compartment was then performed by replacing the PBS with 100μL of RIPA buffer, 1-minute incubation, and then scraping of the cells. Tissue/culture lysates were centrifuged at 10,000 G for 10 minutes at 4°C. Protein concentration was determined using Bradeford essay (BioRad).

Western Blotting

Protein samples were mixed with SDS sample buffer and boiled at 100°C for 10min, and then loaded to 10% acrylamide gels for SDS-PAGE. Proteins were transferred to nitrocellulose membranes in buffer containing 20% MeOH. Membranes were blocked with 5% skim-milk

(BD) or 5% BSA for 1h, followed by ON incubation at 4°C with primary antibodies: mouse anti human TDP-43 (Proteintech, 1:4000), rabbit anti TDP-43 (Proteintech, 1:2000), rabbit anti ERK1/2 (tERK; Sigma, 1:10,000), mouse anti alpha-tubulin (Abcam, 1:5,000), rabbit anti MAP2 (Milipore, 1:1000), mouse anti TAU-5 (Abcam, 1:250). Membranes were then washed with TBST and incubated 2h at RT with secondary HRP antibody (Jackson Laboratories, 1:10,000), or HRP-Goat-IgG2a-anti-mouse (Jackson, 1:20,000; for puromycin blots) washed with TBST and visualized in iBright 1500 ECL imager (Life Technologies) after 5 min incubation with ECL reagents. Quantification was performed using FIJI ImageJ software.

RNA extraction and cDNA synthesis

MN Axonal RNA was extracted from outer compartment of radial MFCs at 14DIV. Axonal RNA was extracted by removing the PBS (from prior wash) from the outer compartment and adding 100µL TRI reagent lysis reagent (Sigma-Aldrich). Inner well was filled with higher volume of PBS to disable the inward flow of lysis reagent towards the inner (soma) compartment and prevent soma contamination. Axons washed off the plate by pipetting the TRI reagent around the outer well for 30 seconds. RNA from somata in the inner compartment was extracted with 100µL TRI reagent, and lysate was collected in a similar manner. cDNA for axon and soma was prepared with High Capacity Reverse Transcription Kit (Thermo; Cat. 4368814).

For SN RNA extraction, SN axoplasm was obtained from 2 adult mice SNs in a tube containing 100µL PBS and protease inhibitors, cut into small pieces and gently squeezed on ice. The axoplasm was then centrifuged at 10,000 G for 10min at 4°C. RNA was extracted using the RNAeasy micro kit (Qiagen) according to manufacturer's protocols.

PCR and RT-qPCR

Reverse Transcription was performed with High-capacity Reverse Transcription cDNA kit using random primers (Thermo Fisher Scientific). Standard PCR was done to test radial chambers axonal purity using KAPA ReadyMix using the following primers:

Standard PCR primers		
Gene	forward primer	Reverse primer
PolB	CCAAGGACAGGAGTGAATGAC	AAGCACAGAGAAGAGGCAATC
ACTB	GTATGGAATCCTGTGGCATC	AAGCACTTGCGGTGCACGAT

qRT-PCR of SN axoplasm was done for the following genes: PolB, mitochondrial-RNR1, Cox4i, ATP5A1 and NDUFA4. Mitochondrial-RNR1 gene was used as a reference gene when calculating ΔCT, as the we aim to quantify relative mRNA levels of nuclear-encoded mitochondrial genes as a part of total axonal mitochondria.

qPCR primers		
Gene	Forward primer	Reverse primer
PolB	CTACAGTCTGTGGCAGTTTCA	TGGCTGTTTGCTGGATTCT
Mito-RNR1	AAACTCAAAGGACTTGGCGGTACTTTATAT	ATACCTTTTTAGGGTTTGCTGAAGATGG
Cox4i	CATTTCTACTTCGGTGTGCCTTCG	GATCAGCGTAAGTGGGGAAAGCAT
ATP5A1	TGTCGGATCTGCTGCCCAAAC	ACGCACACCACGACTCAAGAGC
Ndufa4	CGTATTTATTGGAGCAGGGGGTACTG	GGCTCTGGGTTGTTCTTTCTGTCC

qPCR Sybr-green reactions were performed with PerfeCTa SYBR green FastMix (QuanaBio) in a StepOne Real-Time PCR system (Thermo Fisher Scientific).

Immunofluorescent staining for cryosections

SN and SC sections were prepared from fixating respective tissues in 4% PFA for 16 hours at 4°C, then incubation with 20% sucrose for 16 hours at 4°C, and cryo-embedding in Tissue-Tek OCT compound (Scigen). Tissues were then cryo-sectioned to 10µm thick slices, washed with PBS, followed by permeabilized and blocking in solution containing 10% goat serum, 1mg/mL BSA and 0.1% Triton in PBS for 1h. Later the sections were incubated ON at 4°C with primary antibody rabbit anti TDP-43 (Proteintech, 1:2,000), followed by 2h incubation at RT with secondary antibody (Jackson laboratory, 1:1,000), wash with PBS and mounting with ProLong Gold (Life Technologies) containing DAPI nuclear staining.

Whole mount NMJ staining

Gastrocnemius (GC), Tibialis Anterior (TA) or Extensor Digitorum Longus (EDL) muscles were dissected from adult mice, cleared from connective tissue and kept in 4% PFA until use. Muscles were washed in PBS, stained for post synaptic AChR with αBTX-Atto-633 (Alomone labs) or αBTX-TMR-594 (Sigma) at 1µg/mL for 15 minutes. Next, muscles were permeabilized with ice-cold MeOH at -20°C for 5 minutes, blocked and further permeabilized with 20 mg/mL BSA and 0.4% Triton for 1 hour. Muscle preparations were agitated ON at RT with appropriate antibodies: chicken anti NFH (1:500, abcam), rabbit anti NFH (1:500, Sigma), rabbit anti TDP-43 (proteintech, 1:2,000), rabbit anti Cox4i (1:500, Abcam), rabbit anti ATP5A1 (1:500, Abcam). Next, muscles were incubated with secondary antibodies (1:500-1,000, Jackson laboratories or Invitrogen). Finally, muscles were cut to small vertical pieces and mounted with VectaShield (Vector Laboratories). Cover slides were sealed until use with nail polish.

Immunofluorescent staining for MNs

10DIV TDPΔNLS MNs cultures in MFCs were fixated for 20min in 4% PFA. For $NaAsO_2$ experiment, $NaAsO_2$ (250μM) was applied for 1 hour prior to fixation. MNs were, permeabilized with 0.1% Triton for 30 min, and then blocked for 1 hour with 10% goat serum, 1mg/mL BSA and 0.1% Triton in PBS for 1 hour. Primary antibodes rabbit anti TDP-43 (Proteintech, 1:2,000), mouse anti Puromycin (Millipore, 1:1,000). Antibodies were diluted in blocking solution, and incubated with samples ON at 4°C. Secondary antibodies(Jackson laboratory, 1:1,000) were diluted in blocking solution and incubated with samples for 2 hour incubation at RT. MN Samples were mounted with ProLong Gold DAPI anti-fade reagent(Life Technologies).

Fluorescence microscopy and image analysis

Confocal images were captured using Nikon Ti microscope equipped with a Yokogawa CSU X-1 spinning disc and an Andor iXon897 EMCCD camera controlled by Andor IQ3 software. Phase-contrast movies of muscle contraction were acquired using the same microscope in Epi-mode and images were captured with an Andor Neo sCMOS camera. All live imaging experiments were performed with 5% CO2 and 37°C humidified using in-situ microscope setup.

Co-culture contraction analysis

NMJ activity was assessed by quantifying the percent of innervated and contracting myocytes in co-culture as previously described[32]. Briefly, after 12 days in co-culture, phase-contrast time lapse image series were acquired at a frame rate of 25 frames-per-second (25 FPS) using a X20 air objective. During imaging, cultures were maintained in controlled temperature and CO_2 environment. For obtaining contraction time traces, we used the “Time Series Analyzer V3” plugin for ImageJ, and marked a region of interest on a small, high contrast and mobile region on the muscle, and then obtained the mean values for each time point.

Turbofect Transfection of puromycin resistant muscles

Primary muscle cells were transfected with either PLKO.1 or with PQCXIP-mCherry empty backbone vectors containing Puromycin-N-acetyltansferase (PAC) gene. 150,000 primary myoblasts plated per well were in a matrigel pre-coated 24-well plate. After 4 hours, myoblasts in each well were transfected with 1μg of DNA (PLKO.1 / PQCXIP-mCherry) and 4μL Turbofect transfection reagent (Thermo scientific) prepared in a serum-free medium. Cultures were incubated with transfection reagent for 12 hours in an antibiotic-free BA medium, and then washed with fresh BA medium with 1% P/S. After 4 hours, cultures lifted from the 24-well plated with trypsin-C and plated in the distal compartment MFCs.

O-Propargyl-Puromycin (OPP) labeling of MN culture

OPP was used to label ribosome-nascent polypeptide chains in MN cell bodies, MN axons and in neuromuscular co-cultures. OPP stock (20mM; Life Technologies) was diluted in the appropriate medium to a final concentration of 20μM, and then applied to either proximal / distal compartments of the MFCs to label cell bodies or axons/NMJs, respectively. Cultures were incubated with OPP for 30 minutes, that was chosen as the preferred time point (Sup. Fig. G-I), while the opposite compartment was maintained with higher medium volume to prevent OPP flow and unspecific labeling. Anisomycin (40μM; Sigma) or cyclohexamide (150nM; Sigma) were applied for 30 minutes before OPP was added to cultures, and then together with OPP for validating specific labeling of newly synthesized proteins. Cultures were then washed twice rapidly with cold PBS and fixed with 4% PFA for 15 minutes at RT. Co-cultures were labeled with 0.5μg/mL αBTX-Atto-633 (alomone) for 15 minutes. Cultures were permeabilized with 0.1% Triton in PBS for 30 minutes at RT. ClickIT reaction with either Alexa-488 Picolyl-Azide or Alexa-594 Picolyl-Azide were performed following the protocols supplied by the manufacturer. Cultures were mounted with ProLong Gold Antifade Reagent.

O-Propargyl-Puromycin (OPP) labeling ex-vivo

OPP was used to label protein synthesis in freshly dissected TA/EDL muscles and SNs. Immediately after mice were euthanized, tissues were extracted into 95% O_2 and 5% CO_2 oxygenized-ringer solution containing OPP (20μM). TA/EDL were separated and further dissected into thinner sections prior incubation with OPP. Tissues were incubated with OPP for 35 minutes in 37°C, then washed 3 times with PBS on an orbital shaker and fixed in 4% PFA for 12 hours at 4°C. Sciatic nerves were further incubated with 20% sucrose for additional 12-24 hours at 4°C, and then embedded in Tissue-Tek OCT compound. ClickIT procedure was performed only on 10μm slices sectioned from the first/last 300μm of sciatic nerves. SN sections were collected to Hitobond+ slides (Marienfeld). SN sections were permeabilized with 0.1% triton for 30 minutes followed by 3 PBS washes.

TA/EDL muscles were labeled with 2μg/mL αBTX-Atto-633 (alomone) for 15 minutes and permeabilized with ice-cold MeOH for 5 minutes at -20°C. Muscles were further permeabilized with 0.4% triton in PBS for 1 hours at RT.

ClickIT reaction with either Alexa-488 Picolyl-Azide was performed following the protocols supplied by the manufacturer. Stained SN section were then mounted with ProLong Gold Antifade Reagent. Muscles were either mounted with VectaShield, or proceeded with to standard immunofluorescence labeling protocol.

Preparation of mass spectrometry samples

For preparation of mass spectrometry samples, 30µg axoplasmic protein lysates from WT and TDPΔNLS animals in 10% SDS buffer were precipitated in 80% acetone at -20 °C overnight. Samples were centrifuged at 18,000 x g at 4 °C for 10 min. Protein pellets were washed twice with 80% acetone, air-dried for 10 min and reconstituted in 50µL urea buffer (6 M urea, 2 M thiourea in 10 mM HEPES/KOH, pH 8.0). Samples were reduced and alkylated with 5 mM TCEP and 20 mM CAA at RT for 30 min, followed by digestion with 0.5µg endoproteinase Lys-C (Wako) at RT for 3 h. Samples were diluted fourfold with 50 mM ammionium bicarbonate (ABC) buffer and digested with 0.5µg trypsin (Sigma) at RT overnight. Digestion was stopped by adding 1% formic acid and peptides were desalted using Stop-and-Go extraction tips as described elsewhere [55].

LC-MS/MS analysis and Data Processing

Proteome analyses were performed using an Easy nLC 1000 ultra-high performance liquid chromatography (UHPLC) coupled to a QExactive Plus mass spectrometer (Thermo Fisher Scientific) with the same settings as described before [56]. Acquired MS spectra were correlated to the mouse FASTA databased using MaxQuant (v. 1.5.3.8) and its implemented Andromeda search engine [57] with all parameters set to default. N-terminal acetylation and methionine oxidation were set as variable modifications and cysteine carbamidomethylation was included as a fixed modification. Missing value imputation, statistical analyses and GO annotations were performed in Perseus (v. 1.6.2.3)58 and data were visualized in Instant Clue[58]. Significance cutoff was set to a log2 fold change of at least ± 0.58 and a -log10 p-value of 1.3.

Mitochondria membrane potential measurement

Mitochondrial membrane potential was assessed with Tetramethylrhodamine Ethyl, Ester (TMRE; Thermo Fisher) dye. Cultures were incubated with 20nM TMRE for 30 minutes in CO_2 incubator, then washed 3 times with culture medium. Images of TMRE labeled axons in the distal compartment of MFCs were acquired before and after cultures were treated with Anisomycin (40µM) or $NaAsO_2$ (250µM) in X60 magnification. The volume of medium was kept higher in the proximal compartment to prevent the flow of treatment and ensure cell bodies remain unaffected. The intensity of TMRE fluorescence in axonal mitochondria was measured using FIJI, and the fraction of change post/pretreatment was calculated for each image field.

Mito-KillerRed (MKR) experiments

MKR construct was a kind gift from Prof. Thomas Schwartz (Boston Children's Hospital).

MKR experiments were performed by co-culturing WT MNs and muscles in MFCs. Immediately after their plating, MNs were infected with lentiviral particles containing the MKR

transfer plasmid. WT ChAT^{tdTomato} MNs were used as a negative control in co-cultures without MKR expression. After 12 days in co-culture, upon NMJ formation, co-cultures were labeled with Oregon-Green BAPTA (OGB; life technologies) for 40 minutes. Axons expressing MKR or ChAT^{tdTomato} were tracked until their contact points with muscles in the distal compartment. An ROI was then marked around the axons that overlap with the muscles, which was later frapped with a 560nm laser (100 repeats of 200µS). High-speed image sequences of calcium transients were acquired before and after 560nm laser irradiation, and the percent of change in contraction rate post/pre was calculated for each muscle.

Lentivirus production and infection

Lentivirus particles were used to infect MNs with the MKR gene. We used second generation packaging system. The helper pVSVG and pGag-Pol were gifts from Prof. Eran Bacharach (Tel-Aviv University). For lentiviral production, HEK293-T cells grown on a 60-mm dish. Once 70 to 80% confluence was achieved, cells were transfected with 10 µg of transfer plasmid, 7.5 µg of pGag-Pol, and 2.5 µg of pVSVG. Plasmids were placed in a calcium-phosphate transfection mix (25 mM Hepes, 5 mM KCl, 140 mM NaCl, and 0.75 mM Na_2PO_4 with 125 mM $CaCl_2$) immediately before their addition to cells, in a volume of 0.5 ml per plate. Culture supernatants were harvested 2 days after transfection and concentrated ×10 using PEG Virus Precipitation kit (Abcam). Final pellets were each resuspended in Neurobasal media, aliquoted, and kept in −80°C until use. For transduction of MNs, 2 µL of concentrated lentiviral suspension was used per MFC containing 150,000 MNs. Lentiviral vectors were added 1 to 2 hours after plating MNs and were washed out three times in CNB medium 24 hours later.

Protein synthesis inhibition functional analysis

Analysis of axon degeneration following protein synthesis inhibition was performed by culturing either WT MNs from HB9::GFP embryos, or ΔNLS and control MNs from hTDP43ΔNLS embryos in the proximal compartment of MFC. Once axons have extensively crossed to the distal compartment, or after 10 days (for hTDP43ΔNLS cultures), protein synthesis inhibitors were added to the distal (axonal) compartment while maintaining a higher volume of medium in the proximal compartment to prevent exposure of the cell-bodies to inhibitors. Puromycin (100µg/mL) or Anisomycin (40µM; only for HB9::GFP MN) were applied exclusively to axons in CNB medium. Images of axons were acquired at low magnification before, and after 16 (hTDP43ΔNLS) and 24 hours to monitor the extent of axon degeneration. Analysis of NMJ function following protein synthesis inhibition with puromycin was performed by co-culturing WT MNs with primary muscles transfected with empty PQCXIP-mCherry vectors expressing PAC gene for puromycin resistance. After 12 days in co-culture, once

cultures matured and NMJ were formed, Puromycin (100µg/mL) was added exclusively to the distal (NMJ) compartment for 16 hours. The proximal compartment was kept with higher volume of medium for allowing puromycin to act only locally within the NMJ compartment. After 16 hours, cultures were labeled with OGB, and the calcium activity of axons and muscles was recorded. Analysis of the percent of muscles with calcium transients in co-culture, was performed on muscles with at least one overlapping axon. Only muscles that expressed mCherry (as a reporter for the expression of PAC) were used for this analysis.

Co-culture calcium imaging

OGB lyophilized stock (Life technologies) was resuspended with 20% (w/v) Pluronic acid for a stock concentration of 3mM Stock was diluted 1:1,000 in the appropriate medium. OGB was incubated with cultures for 40 minutes in 37°C, 5% CO_2 incubator, and then washed 3 times with culture medium prior imaging. Calcium transients in axons and muscles were recorded in a spinning disk confocal microscope equipped with an EMCCD camera with X40 oil objective using 488nm laser. Image sequences of 1,000 frames were acquired at frame rate of 25 FPS. Image analysis was performed using the "Time Series Analyzer V3" plugin for FIJI. Briefly, the mean OGB values for a Region of Interest (ROI) were plotted over the complete movie length. This assisted us to determine whether or not a certain muscle was active, and whether the activity was paired with neuronal firing. For figure labeling, axon endings on muscles, which also had high basal OGB signal were considered as NMJs.

Statistical analysis

Statistical parameters and test used are noted in Figure legends. Threshold for determining statistical significance was $P < 0.05$. All statistical analysis was performed with Graph-pad Prism 7.

Acknowledgment:

The authors declare no conflict of interest. We thank M. Fainzilber and E. Hornstein for helpful comments on the manuscript. This work was supported by the ISF (Israel Science foundation) and Ministry of Science and Technology State of Israel, grants, 735/19, and 0601166782 respectively.

References

1. Taylor, J. P., Brown, R. H. & Cleveland, D. W. Decoding ALS: from genes to mechanism. *Nature* **539**, 197–206 (2016).
2. Cook, C. & Petrucelli, L. Genetic Convergence Brings Clarity to the Enigmatic Red Line in ALS. *Neuron* **101**, 1057–1069 (2019).
3. Neumann, M. *et al.* Ubiquitinated TDP-43 in frontotemporal lobar degeneration and amyotrophic lateral sclerosis. *Science (80-.).* **314**, 130–133 (2006).
4. Melamed, Z. *et al.* Premature polyadenylation-mediated loss of stathmin-2 is a hallmark of TDP-43-dependent neurodegeneration. *Nat. Neurosci.* **22**, 180–190 (2019).
5. Tsuji, H. *et al.* Molecular analysis and biochemical classification of TDP-43 proteinopathy. *Brain* **135**, 3380–3391 (2012).
6. Barmada, S. J. *et al.* Cytoplasmic mislocalization of TDP-43 is toxic to neurons and enhanced by a mutation associated with familial amyotrophic lateral sclerosis. *J. Neurosci.* **30**, 639–649 (2010).
7. Klim, J. R. *et al.* ALS-implicated protein TDP-43 sustains levels of STMN2, a mediator of motor neuron growth and repair. *Nat. Neurosci.* **22**, 167–179 (2019).
8. Chou, C. C. *et al.* TDP-43 pathology disrupts nuclear pore complexes and nucleocytoplasmic transport in ALS/FTD. *Nat. Neurosci.* **21**, 228–239 (2018).
9. Ling, J. P., Pletnikova, O., Troncoso, J. C. & Wong, P. C. TDP-43 repression of nonconserved cryptic exons is compromised in ALS-FTD. *Science (80-.).* **349**, 650–655 (2015).
10. Kabashi, E. *et al.* TARDBP mutations in individuals with sporadic and familial amyotrophic lateral sclerosis. *Nat. Genet.* **40**, 572–574 (2008).
11. Suk, T. R. & Rousseaux, M. W. C. The role of TDP-43 mislocalization in amyotrophic lateral sclerosis. *Mol. Neurodegener.* **15**, 1–16 (2020).
12. Chen, Y. & Cohen, T. J. Aggregation of the nucleic acid– binding protein TDP-43 occurs via distinct routes that are coordinated with stress granule formation. *J. Biol. Chem.* **294**, 3696–3706 (2019).
13. Russo, A. *et al.* Increased cytoplasmic TDP-43 reduces global protein synthesis by interacting with Rack1 on polyribosomes. *Hum. Mol. Genet.* **26**, 1407–1418 (2017).
14. Gasset-Rosa, F. *et al.* Cytoplasmic TDP-43 De-mixing Independent of Stress Granules Drives Inhibition of Nuclear Import, Loss of Nuclear TDP-43, and Cell Death Article Cytoplasmic TDP-43 De-mixing Independent of Stress Granules Drives Inhibition of Nuclear Import, Loss of Nuclear TDP-43, and Cell Death. *Neuron* **102**, 339–357 (2019).
15. Alami, N. H. *et al.* Axonal Transport of TDP-43 mRNA Granules Is Impaired by ALS-

Causing Mutations. *Neuron* **81**, 536–543 (2014).

16. Gopal, P. P., Nirschl, J. J., Klinman, E. & Holzbaurb, E. L. F. Amyotrophic lateral sclerosis-linked mutations increase the viscosity of liquid-like TDP-43 RNP granules in neurons. *Proc. Natl. Acad. Sci. U. S. A.* **114**, E2466–E2475 (2017).
17. Liao, Y. C. *et al.* RNA Granules Hitchhike on Lysosomes for Long-Distance Transport, Using Annexin A11 as a Molecular Tether. *Cell* **179**, 147-164.e20 (2019).
18. Sahoo, P. K. *et al.* Axonal G3BP1 stress granule protein limits axonal mRNA translation and nerve regeneration. *Nat. Commun.* **9**, 1–14 (2018).
19. Costa, C. J. & Willis, D. E. To the end of the line: Axonal mRNA transport and local translation in health and neurodegenerative disease. *Dev. Neurobiol.* **78**, 209–220 (2018).
20. Terenzio, M. *et al.* Locally translated mTOR controls axonal local translation in nerve injury. *Science (80-.).* **359**, 1416–1421 (2018).
21. Cioni, J.-M. *et al.* Late Endosomes Act as mRNA Translation Platforms and Sustain Mitochondria in Axons Article Late Endosomes Act as mRNA Translation Platforms and Sustain Mitochondria in Axons. *Cell* **176**, 56–72 (2019).
22. Hafner, A. S., Donlin-Asp, P. G., Leitch, B., Herzog, E. & Schuman, E. M. Local protein synthesis is a ubiquitous feature of neuronal pre- And postsynaptic compartments. *Science (80-.).* **364**, (2019).
23. Shigeoka, T. *et al.* Dynamic Axonal Translation in Developing and Mature Visual Circuits. *Cell* **166**, 181–192 (2016).
24. López-Erauskin, J. *et al.* ALS/FTD-Linked Mutation in FUS Suppresses Intra-axonal Protein Synthesis and Drives Disease Without Nuclear Loss-of-Function of FUS. *Neuron* **100**, 816-830.e7 (2018).
25. Zhang, Y. J. *et al.* Poly(GR) impairs protein translation and stress granule dynamics in C9orf72-associated frontotemporal dementia and amyotrophic lateral sclerosis. *Nat. Med.* **24**, 1136–1142 (2018).
26. Dadon-Nachum, M., Melamed, E. & Offen, D. The “Dying-Back” Phenomenon of Motor Neurons in ALS. *J. Mol. Neurosci.* **43**, 470–477 (2011).
27. So, E. *et al.* Mitochondrial abnormalities and disruption of the neuromuscular junction precede the clinical phenotype and motor neuron loss in hFUSWT transgenic mice. *Hum. Mol. Genet.* **27**, 463–474 (2018).
28. Zahavi, E. E. *et al.* A compartmentalized microfluidic neuromuscular co-culture system reveals spatial aspects of GDNF functions. *J. Cell Sci.* **128**, 1241–1252 (2015).
29. Maimon, R. *et al.* Mir126-5p downregulation facilitates axon degeneration and nmj disruption via a non–cell-autonomous mechanism in ALS. *J. Neurosci.* **38**, 5478–5494

(2018).

30. Ionescu, A. *et al.* Targeting the Sigma-1 Receptor via Pridopidine Ameliorates Central Features of ALS Pathology in a SOD1G93A Model. *Cell Death Dis.* **10**, 210 (2019).
31. Altman, T., Geller, D., Kleeblatt, E., Gradus-Perry, T. & Perlson, E. An in vitro compartmental system underlines the contribution of mitochondrial immobility to the ATP supply in the NMJ. *J. Cell Sci.* **132**, (2019).
32. Ionescu, A., Zahavi, E. E., Gradus, T., Ben-Yaakov, K. & Perlson, E. Compartmental microfluidic system for studying muscle-neuron communication and neuromuscular junction maintenance. *Eur. J. Cell Biol.* **95**, 69–88 (2016).
33. Ionescu, A. & Perlson, E. Patient-derived co-cultures for studying ALS. *Nature Biomedical Engineering* **3**, 13–14 (2019).
34. Osaki, T., Uzel, S. G. M. & Kamm, R. D. Microphysiological 3D model of amyotrophic lateral sclerosis (ALS) from human iPS-derived muscle cells and optogenetic motor neurons. *Sci. Adv.* **4**, 5847 (2018).
35. Ionescu, A. *et al.* Targeting the Sigma-1 Receptor via Pridopidine Ameliorates Central Features of ALS Pathology in a SOD1 G93A Model. *Cell Death Dis.* **10**, (2019).
36. Zahavi, E. E. *et al.* A compartmentalized microfluidic neuromuscular co-culture system reveals spatial aspects of GDNF functions. *J. Cell Sci.* **128**, 1241–1252 (2015).
37. Walker, A. K. *et al.* Functional recovery in new mouse models of ALS/FTLD after clearance of pathological cytoplasmic TDP-43. *Acta Neuropathol.* **130**, 643–660 (2015).
38. Spiller, K. J. *et al.* Selective motor neuron resistance and recovery in a new inducible mouse model of TDP-43 proteinopathy. *J. Neurosci.* **36**, 7707–7717 (2016).
39. Spiller, K. J. *et al.* Microglia-mediated recovery from ALS-relevant motor neuron degeneration in a mouse model of TDP-43 proteinopathy. *Nat. Neurosci.* **21**, 329–340 (2018).
40. Rangaraju, V., Lauterbach, M. & Schuman, E. M. Spatially Stable Mitochondrial Compartments Fuel Local Translation during Plasticity. *Cell* **176**, 73-84.e15 (2019).
41. Calvo, S. E., Clauser, K. R. & Mootha, V. K. MitoCarta2.0: An updated inventory of mammalian mitochondrial proteins. *Nucleic Acids Res.* **44**, D1251–D1257 (2016).
42. Farias, J., Holt, C. E., Sotelo, J. R. & Sotelo-Silveira, J. R. Axon micro-dissection and transcriptome profiling reveals the in vivo RNA content of fully differentiated myelinated motor axons. *RNA* rna.073700.119 (2020). doi:10.1261/rna.073700.119
43. Maciel, R. *et al.* The human motor neuron axonal transcriptome is enriched for transcripts related to mitochondrial function and microtubule-based axonal transport. *Exp. Neurol.* **307**, 155–163 (2018).

44. Fallini, C., Bassell, G. J. & Rossoll, W. The ALS disease protein TDP-43 is actively transported in motor neuron axons and regulates axon outgrowth. *Hum. Mol. Genet.* **21**, 3703–3718 (2012).
45. Briese, M. *et al.* Loss of Tdp-43 disrupts the axonal transcriptome of motoneurons accompanied by impaired axonal translation and mitochondria function. *Acta Neuropathol. Commun.* **8**, 116 (2020).
46. Nagano, S. *et al.* TDP-43 transports ribosomal protein mRNA to regulate axonal local translation in neuronal axons. *Acta Neuropathol.* **1**, 3 (2020).
47. Khalfallah, Y. *et al.* TDP-43 regulation of stress granule dynamics in neurodegenerative disease-relevant cell types /631/80/304 /631/378/87 /13/1 /13/31 /13/51 /13/109 /13/106 /13/89 /14/19 /14/32 /82/80 article. *Sci. Rep.* **8**, 1–13 (2018).
48. Lee, C. W. & Peng, H. B. Mitochondrial clustering at the vertebrate neuromuscular junction during presynaptic differentiation. *J. Neurobiol.* **66**, 522–536 (2006).
49. Misgeld, T., Kerschensteiner, M., Bareyre, F. M., Burgess, R. W. & Lichtman, J. W. Imaging axonal transport of mitochondria in vivo. *Nat. Methods* **4**, 559–561 (2007).
50. Kuzniewska, B. *et al.* Mitochondrial protein biogenesis in the synapse is supported by local translation. *EMBO Rep.* **21**, (2020).
51. Altman, T. & Perlson, E. Neuromuscular junction mitochondrial enrichment: a “double-edged sword” underlying the selective motor neuron vulnerability in amyotrophic lateral sclerosis. *Neural Regen. Res.* **16**, 115 (2021).
52. Brooks, B. R. El escorial World Federation of Neurology criteria for the diagnosis of amyotrophic lateral sclerosis. *J. Neurol. Sci.* **124**, 96–107 (1994).
53. Altman, T., Maimon, R., Ionescu, A., Pery, T. G. & Perlson, E. Axonal transport of organelles in motor neuron cultures using microfluidic chambers system. *J. Vis. Exp.* **2020**, 60993 (2020).
54. Gluska, S., Chein, M., Rotem, N., Ionescu, A. & Perlson, E. Tracking Quantum-Dot labeled neurotropic factors transport along primary neuronal axons in compartmental microfluidic chambers. *Methods Cell Biol.* **131**, 365–87 (2016).
55. Rappsilber, J., Ishihama, Y. & Mann, M. Stop and Go Extraction Tips for Matrix-Assisted Laser Desorption/Ionization, Nanoelectrospray, and LC/MS Sample Pretreatment in Proteomics. *Anal. Chem.* **75**, 663–670 (2003).
56. Nolte, H., Hölper, S., Selbach, M., Braun, T. & Krüger, M. Assessment of Serum Protein Dynamics by Native SILAC Flooding (SILflood). *Anal. Chem.* **86**, 11033–11037 (2014).
57. Cox, J. *et al.* Andromeda: A Peptide Search Engine Integrated into the MaxQuant Environment. *J. Proteome Res.* **10**, 1794–1805 (2011).
58. Nolte, H., MacVicar, T. D., Tellkamp, F. & Krüger, M. Instant Clue: A Software Suite

for Interactive Data Visualization and Analysis. *Sci. Rep.* **8**, 12648 (2018).

Figure Legends

Figure 1 – TDP-43 mislocalizes to distal MN axons in ALS patients and TDPΔNLS mice: **A)** Schematic of the experimental setup for muscle punch biopsies to identify intra-muscular nerves. **B and D)** Representative immunofluorescence images of non-ALS and ALS patient intra-muscular nerves. Neurofilament (NFH)-red. In **B** - total TDP-43 (tTDP)-green. In **D** - phosphorylated TDP-43 (pTDP)-green. Scale bar = 10μm. **C and E)** Quantification of tTDP-43 (C) or pTDP (E) signal within NFH positive axons, normalized to NFH. Error bars represent S.D. **In C** - n=31 images (5 non-ALS) and 21 images (3 ALS) of intra-muscular nerves. *P=0.011, unpaired t test. **In E** - n=30 images (5 non-ALS) and 23 images (3 ALS). **P<0.01, unpaired t test. **F)** Schematic illustration of the structure of radial MFCs for large scale purification of MN axons. MNs are plated in a round well in the middle and extend their axons through microgrooves (green, HB9::GFP axons). Lower panel: Western blot analysis of purified TDPΔNLS MN axons and soma with (control) or without dox (ΔNLS), immunoblotted with antibodies for human TDP-43 (hTDP43, upper panel) and total TDP-43 (tTDP-43, middle panel). ERK 1/2 was used as a loading control (lower panel). **G)** Quantification of purified axonal tTDP-43 bands normalized to tERK in TDPΔNLS MN with (control) or without dox (ΔNLS). Values are shown as a fold change from control. n=3 experiments for each group, error bar represents S.E.M. *P=0.047, paired t test. **H)** Western blot analysis of sciatic nerve (SN) axoplasm with antibodies for hTDP43 and tTDP-43. ERK 1/2 was used as a loading control. **I)** Representative images of ChAT::Rosa TDPΔNLS mice and LM control sciatic nerves stained with tTDP-43 antibody (green). Red indicates $ChAT^{tdTomato}$ positive MN axons. Scale bar = 10μm. **J)** Quantification of tTDP-43 signal within $ChAT^{tdTomato}$ axons. n=50 and 48 images analyzed from 3 LM and 3 TDPΔNLS mice SNs, respectively. Error bars represent S.D. ****P<0.0001, unpaired t test. **K)** Representative images of TDPΔNLS mice GC muscle NMJ before and two weeks after dox retraction, stained with tTDP-43 antibody (green), Bungarotoxin (grey) and NFH (red). TDP-43-NFH colocalization panel (yellow) shows the 3D colocalization. Scale bar = 10μm.

Figure 2 – Axonal TDP-43 accumulation leads to formation of RNP granules positive for the SG marker G3BP1 and RNA: **A**) Representative images, **B**) co-localization profiles and **C-E**) quantification of Chat::Rosa-TDPΔNLS MN axons (red) with (control) or without dox (ΔNLS),

immunostained for TDP-43 (green) and G3BP1 (magenta). Scale bar = 10μm **C)**, % of TDP-43/G3BP1 colocalized area from total axon area**, D)** Average axonal G3BP1 intensity and **E)** TDP-43 intensity were measured. n=22 and 26 axons for control and ΔNLS, respectively. Unpaired t-test, ****p<0.0001, ***p<0.001. **F**) Representative images, **G)** co-localization profiles, and **H)** quantification of TDPΔNLS MN axons with (control) or without dox (ΔNLS), immunostained for TDP-43 (green) and G3BP1 (magenta) and dyed with Syto-RNA (red). Scale bar = 10μm. In **H**, total area of TDP-43-G3BP1-SytoRNA colocalized area was calculated and compared to total axon area. n=28 and 35 axons for control and ΔNLS, respectively. Unpaired t-test, ****p<0.0001.

Figure 3 - TDP-43 axonal accumulation leads to reduction of local protein synthesis in MN axons and NMJs. **A)** Representative images and **B)** quantification of OPP puncta density in distal MN from TDPΔNLS axons with (control) and without dox (ΔNLS). Scale bar = 5μm. n=100, 112 axons. Unpaired two-tail student's t-test ****p<0.0001. **C)** Representative images and **D)** quantification of OPP puncta density in *in-vitro* NMJs from TDPΔNLS MN axons with (control) and without dox (ΔNLS). Scale bar = 5μm. Data is shown as the mean ± SEM. n=3 average of 3 independent repeats, unpaired two-tail student's t-test **p<0.01. **E)** Representative images and **F)** quantification of OPP labeled SN sections shows OPP labeling in ChAT:Rosa^{tdTomato} MN axons of TDPΔNLS mice compared to LM control mice. Scale bar = 10μm. Data is shown as the mean ± S.E. n=3 the averages of 3 independent repeats from 3 mice in each condition. *p<0.05 unpaired two-tail student's t-test. **G)** Representative images and **H)** quantification of pre-synaptic axons (ChAT:Rosa^{tdTomato}) in TA muscle NMJs. Scale bar = 10μm. Data is shown as the mean ± SD. n=24, 19 NMJs from 3 mice of each condition. Unpaired two-tail student's t-test **p<0.01.

Figure 4 - TDP-43 Axonal Accumulation Reduces Levels of Nuclear-Encoded Mitochondrial Proteins and Decreases Mitochondria-Associated local synthesis. **A)** Volcano plot representing SN proteome analysis of TDPΔNLS and LM mice. Data is shown as Log_2FC of TDPΔNLS over LM proteome. n=4 sciatic nerve axoplasm preparations from each condition. Nuclear-encoded mitochondrial proteins marked in blue (Mitocarta). Cox4i1 and ATP5A1 (labeled orange) were chosen for further characterization. **B)** Venn diagram comparing all mitocarta proteins in our dataset with proteins that were up-regulated (upper panel) or down-regulated (lower panel). $Log_2FC>1$ for up-regulated and <-1 for down-regulated proteins. **C)** GO analyses categories of proteome results. Blue indicates down-regulated proteins, red up-regulated. **D)** qRT-PCR of nuclear-encoded mitochondria protein mRNA levels in SN axoplasm from TDPΔNLS and LM mice. mRNA levels were normalized to total mitochondria content, as measured by mitochondria-encoded mRNA, RNR2. PolB mRNA was measured

to identify no contamination of nuclear RNA. n=3, 3 SNs. One-way Anova with Holm-Sidak correction revealed no significant differences. **E)** Representative images and **F)** quantification of OPP (red) and mitotracker (green) colocalization in distal axons. The percent of mitochondria in colocalization with OPP in distal axons in ΔNLS axons compared with control axons. Data is shown as the mean percent of mito-OPP colocalization ± SD. Scale bar = 5μm. n=43 (control), 36 (ΔNLS) axons from 3 independent repeats. Unpaired two-tail student's t-test ***p>0.001. **G)** Representative images and **H)** quantification of TMRE signal in control axons (n=40), in axons treated with protein synthesis inhibitor anisomycin (n=69) or treated with $NaAsO_2$ (n=43). Scale bar =10μm. Data is shown as the mean TMRE signal. One-way ANOVA with Holm-Sidak correction ***p<0.001. **I)** Representative images **J)** and quantification of TMRE signal in ΔNLS and control MN axons cultured in MFC. Protein synthesis of distal axons was transiently inhibited for 4 hours and then washed out. Axons were left to recover for 24 hours, after which TMRE signal was collected from distal axons. Data is shown as the mean percent of TMRE signal post/pre protein synthesis inhibitors ± SD. n=32 ,29 axons. unpaired two-tail student's t-test ****p<0.0001.

Figure 5 – NMJ function is dependent on mitochondria and local synthesis, and their absence leads to decreased NMJ activity and axon degeneration. **A)** Schematic illustration of Mito-Killer-Red (MKR) experimental setup. MNs are cultured in MFCs and induced to express MKR using lentiviral infection. Myocytes are plated on the distal compartment of MFC. MKR is bleached at the NMJ with a 560nm laser leading to mitochondrial damage. **B)** Representative images of MKR (red) in pre-synaptic axons before, and after bleach (white dashed line indicates bleached region). Lower panel depicts a muscle and its innervating axon, all visualized by Oregon-Green BAPTA (OGB), which was also used for measuring the calcium transients in muscles before and after MKR activation. **C-D)** Time traces of the OGB intensity indicating muscle contraction (**C**) and quantification (**D**) of contraction ratio before and after MKR pre-synaptic bleaching (n=13). Bleaching pre-synaptic axons expressing ChAT:RosatdTomato and not MKR served as a control (n=12). Scale bar = 10μm. Data is shown as the mean ± S.D. unpaired two-tail student's t-test ****p<0.0001. **E)** Schematic illustration of experimental procedure. Healthy MNs were co-cultured with muscles that were pre-transfected with PQCXIP-mCherry empty vectors expressing puromycin-resistance gene (PAC). Upon NMJ maturation, Puromycin (100μg/mL) was added exclusively to the NMJ compartment for 16 hours before labeling of the co-cultures with OGB, and imaging. **F)** Left panel: Representative images from time series movies of calcium indicator OGB-labeled co-cultures. Right panel: The images demonstrate paired axon-muscle calcium activity only in control NMJs, but not in co-cultures treated distally with puromycin (100μg/mL), the pre-synaptic calcium release does not translate into efficient neurotransmission. Scale bar: 20μm.

G) Representative time traces of calcium activity in pre-synaptic neurons and post-synaptic muscles show paired activity in control cultures (upper plot), and unpaired activity in puromycin-treated cultures (lower plot). **H)** Quantitative analysis of the percent of innervated and contracting muscles after inhibition of axonal and pre-synaptic local synthesis. n=7 (control) and 9 (puro) MFC co-cultures from 3 independent experiments, ****p<0.0001 unpaired two-tail student's t-test. **I)** Representative images and **J)** quantification of the percent of degenerating axons in the distal compartment of ΔNLS and control MN axons following 16 and 24h of puromycin treatment. Scale bar = 50μm. Data is shown as the mean percent of degenerating axons (length) per total axons (length) in MFC ± S.D. n = 4 (control) MFCs, and 3 (ΔNLS) MFCs, all from 3 independent repeats. One-way ANOVA with Holm-Sidak correction *p<0.05.

Figure 6 - Restoring TDP-43 localization recovers local translation of mitochondrial proteins in distal axons and the NMJs, and enables functional reinnervation. **A)** Western-blot image (upper panel) and quantification (lower panel) of mice sciatic nerves (SNs) from LM, TDPΔNLS, and TDPΔNLS after dox re-application (recovery), blotted for total-TDP-43 (tTDP-43) and human-TDP-43 (hTDP-43). tERK used as a loading control. Signal calculated as the tTDP-43 signal normalized to the tERK signal. Data is shown as the mean ± S.E. n=3 SN axoplasm preparations, one-way ANOVA with Holm-Sidak correction, *p<0.05, **p<0.01. **B)** Representative images and **C)** quantification of TDP-43 (green) immunolabeled $ChAT^{tdTomato}$-TDPΔNLS (Chat-red) SN sections from LM (control), ΔNLS, and Recovery (Rec.) mice. Scale bar = 20μm. Data is shown as the mean tTDP-43 intensity in SN ± S.D. n=34 (control), 34 (ΔNLS), 33 (rec) SN sections imaged from 3 mice in each condition. One-way ANOVA with Holm-Sidak correction *p<0.05, ***p<0.001. **D)** Representative images of NMJ labeling for TDP-43 (green) with postsynaptic BTX (red) and pre-synaptic NFH (grey), and **E)** quantification of the percent of NMJs with apparent TDP-43 aggregates. Scale bar = 10μm. Data is shown as the mean ± SE. n=3 mice from each condition. Unpaired two-tailed student's t-test ***p<0.001. **F)** Representative images and **G)** analysis of the OPP puncta density in NMJs from TDPΔNLS MNs without dox (ΔNLS) and with dox reintroduction (Recovery) and with constant dox application (Cont.). Scale bar = 5μm. Data is shown as the mean number of OPP puncta/μm ± S.E. n=3 average of 3 independent biological repeats, one-way ANOVA with Holm-Sidak correction, ***p<0.001. **H)** Representative images and **I)** analysis of the OPP labeling intensity in pre-synaptic compartment in NMJs of TA muscle from LM n=32 NMJs, ΔNLS n=30 NMJs, and recovery mice n=39,NMJs. All from 3 mice. Data is shown as the mean OPP-ChAT colocalization intensity ± S.D. Scale bar = 10μm. One-way ANOVA with Holm-Sidak correction, *p<0.05, ***p<0.001. **J)** Representative co-localization images of mitochondria protein Cox4i (green) with pre-synaptic ChAT (red) and OPP labeling (gray) in

NMJs from LM, ΔNLS, and recovered mice. Scale bar = 10μm. **K)** Representative histogram of Cox4i (red) and OPP (green) signals within NMJ pre-synapse. **L)** Quantitative colocalization analysis of the percent of Cox4i area within the pre-synapse area ($ChAT^{tdTomato}$) in LM, ΔNLS, and recovered mice. Data is shown as the mean percent of Cox4i-ChAT colocalization ± S.D. n=21, 23, 13 NMJs. 3 mice from each group. One-way ANOVA with Holm-Sidak correction, ****p<0.0001, ***p<0.001. **M)** Quantitative analysis of Cox4i colocalization with OPP in the pre-synaptic NMJ ($ChAT^{tdTomato}$) from LM, ΔNLS, and recovered mice. Data is shown as the mean percent of Cox4i-OPP colocalization area ± S.D. n=21, 23, 13 NMJs from 3 mice of each group. One-way ANOVA with Holm-Sidak correction, ***p<0.001, **p<0.01. **N)** Representative images and **O)** quantification of *in-vitro* NMJ innervation by structural (measured as the percent of $ChAT^{tdTomato}$ positive BTX clusters) and **P)** functional aspects (measured as the percent of innervated and contracting muscles from total innervated muscles). NMJ re-innervation was measured in control, ΔNLS and recovery co-cultures. Scale bar = 40μm in large image, 5μm in inset. Data is shown as the mean ± S.E. For **I**, n=3,3,3 MFCs for each condition. For K, n=7,6,7 MFCs. Both from 3 independent repeats. One-way ANOVA with Holm-Sidak correction, *p<0.05, **p<0.01, ***p<0.001. **Q)** Representative images of NMJs from LM, ΔNLS, and recovered mice. Scale bar = 10μm. **R)** Quantification of the percentage of innervated NMJs in $ChAT^{tdTomato}$-LM, TDPΔNLS and Recovery mice calculated as percent of NMJs with BTX (post-synaptic) colocalization with Chat signal (pre-synaptic). Data is shown as the mean ± S.E. n=3 mice from each condition. One-way ANOVA with Holm-Sidak correction *p<0.05.

Figure 7 – Model: TDP-43 axonal mislocalization creates RNPs which decrease local translation of nuclear-encoded mitochondrial proteins, leading to NMJ degeneration. **a)** TDP-43 is regularly found in axons and NMJs in controlled amounts and supports axonal and synaptic local translation by shuttling mRNAs. **b-c)** Cytoplasmic mislocalization of TDP-43 in ALS **(b)** promotes its axonal accumulation in RNP condensates that sequester mRNAs and interferes with local translation, especially of nuclear-encoded mitochondrial proteins **(c)**. This process leads to synaptic mitochondria toxicity and eventually to NMJ dysfunction and degeneration **(d)**.

Figures

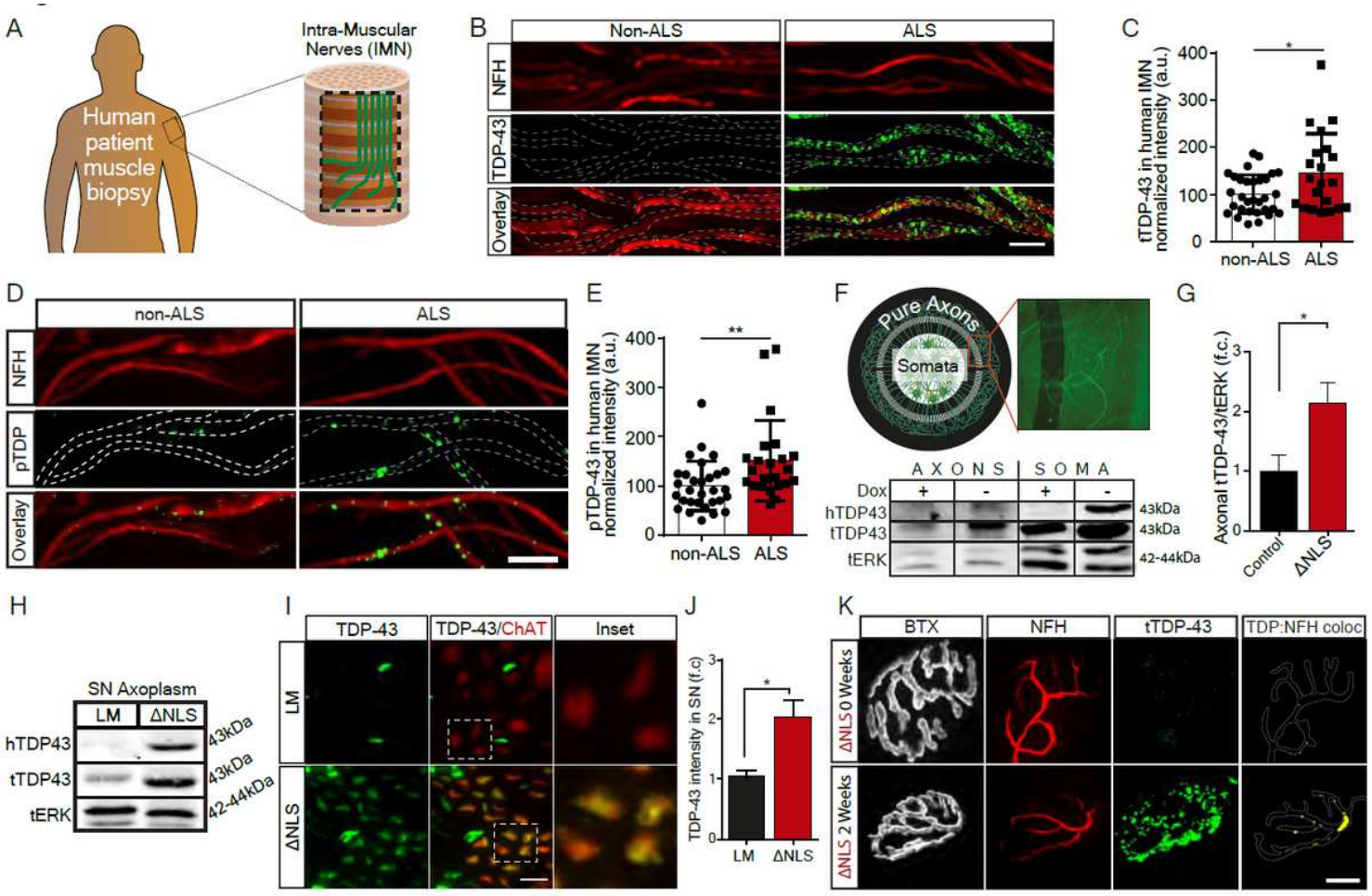

Figure 1

TDP-43 mislocalizes to distal MN axons in ALS patients and TDPΔNLS mice: A) Schematic of the experimental setup for muscle punch biopsies to identify intra-muscular nerves. B and D) Representative immunofluorescence images of non-ALS and ALS patient intra-muscular nerves. Neurofilament (NFH)-red. In B - total TDP-43 (tTDP)-green. In D - phosphorylated TDP-43 (pTDP)-green. Scale bar = 10μm. C and E) Quantification of tTDP-43 (C) or pTDP (E) signal within NFH positive axons, normalized to NFH. Error bars represent S.D. In C - n=31 images (5 non-ALS) and 21 images (3 ALS) of intra-muscular nerves. *P=0.011, unpaired t test. In E - n=30 images (5 non-ALS) and 23 images (3 ALS). **P<0.01, unpaired t test. F) Schematic illustration of the structure of radial MFCs for large scale purification of MN axons. MNs are plated in a round well in the middle and extend their axons through microgrooves (green, HB9::GFP axons). Lower panel: Western blot analysis of purified TDPΔNLS MN axons and soma with (control) or without dox (ΔNLS), immunoblotted with antibodies for human TDP-43 (hTDP43, upper panel) and total TDP-43 (tTDP-43, middle panel). ERK 1/2 was used as a loading control (lower panel). G) Quantification of purified axonal tTDP-43 bands normalized to tERK in TDPΔNLS MN with (control) or without dox (ΔNLS). Values are shown as a fold change from control. n=3 experiments for each group, error bar represents S.E.M. *P=0.047, paired t test. H) Western blot analysis of sciatic nerve (SN)

axoplasm with antibodies for hTDP43 and tTDP-43. ERK 1/2 was used as a loading control. I) Representative images of ChAT::Rosa TDPΔNLS mice and LM control sciatic nerves stained with tTDP-43 antibody (green). Red indicates ChATtdTomato positive MN axons. Scale bar = 10μm. J) Quantification of tTDP-43 signal within ChATtdTomato axons. n=50 and 48 images analyzed from 3 LM and 3 TDPΔNLS mice SNs, respectively. Error bars represent S.D. ****P<0.0001, unpaired t test. K) Representative images of TDPΔNLS mice GC muscle NMJ before and two weeks after dox retraction, stained with tTDP-43 antibody (green), Bungarotoxin (grey) and NFH (red). TDP-43-NFH colocalization panel (yellow) shows the 3D colocalization. Scale bar = 10μm.

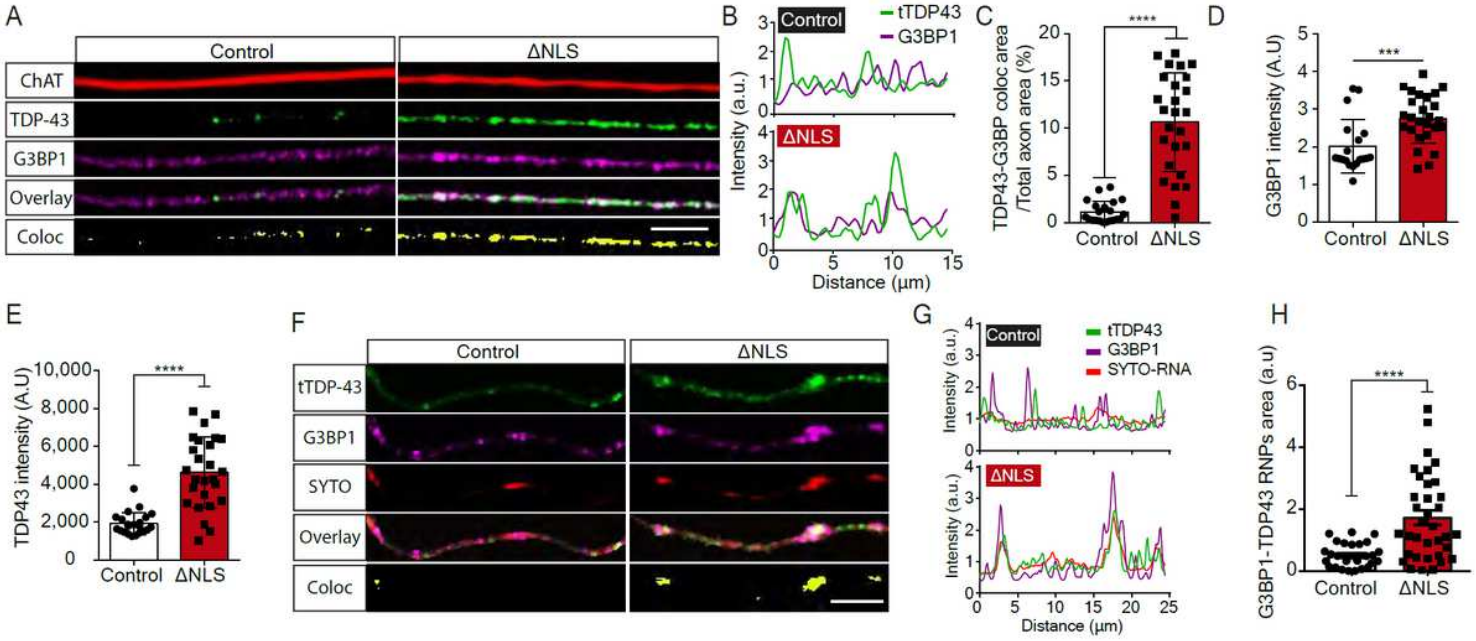

Figure 2

Axonal TDP-43 accumulation leads to formation of RNP granules positive for the SG marker G3BP1 and RNA: A) Representative images, B) co-localization profiles and C-E) quantification of Chat::Rosa-TDPΔNLS MN axons (red) with (control) or without dox (ΔNLS), immunostained for TDP-43 (green) and G3BP1 (magenta). Scale bar = 10μm C), % of TDP-43/G3BP1 colocalized area from total axon area, D) Average axonal G3BP1 intensity and E) TDP-43 intensity were measured. n=22 and 26 axons for control and ΔNLS, respectively. Unpaired t-test, ****p<0.0001, ***p<0.001. F) Representative images, G) co-localization profiles, and H) quantification of TDPΔNLS MN axons with (control) or without dox (ΔNLS), immunostained for TDP-43 (green) and G3BP1 (magenta) and dyed with Syto-RNA (red). Scale bar = 10μm. In H, total area of TDP-43-G3BP1-SytoRNA colocalized area was calculated and compared to total axon area. n=28 and 35 axons for control and ΔNLS, respectively. Unpaired t-test, ****p<0.0001.

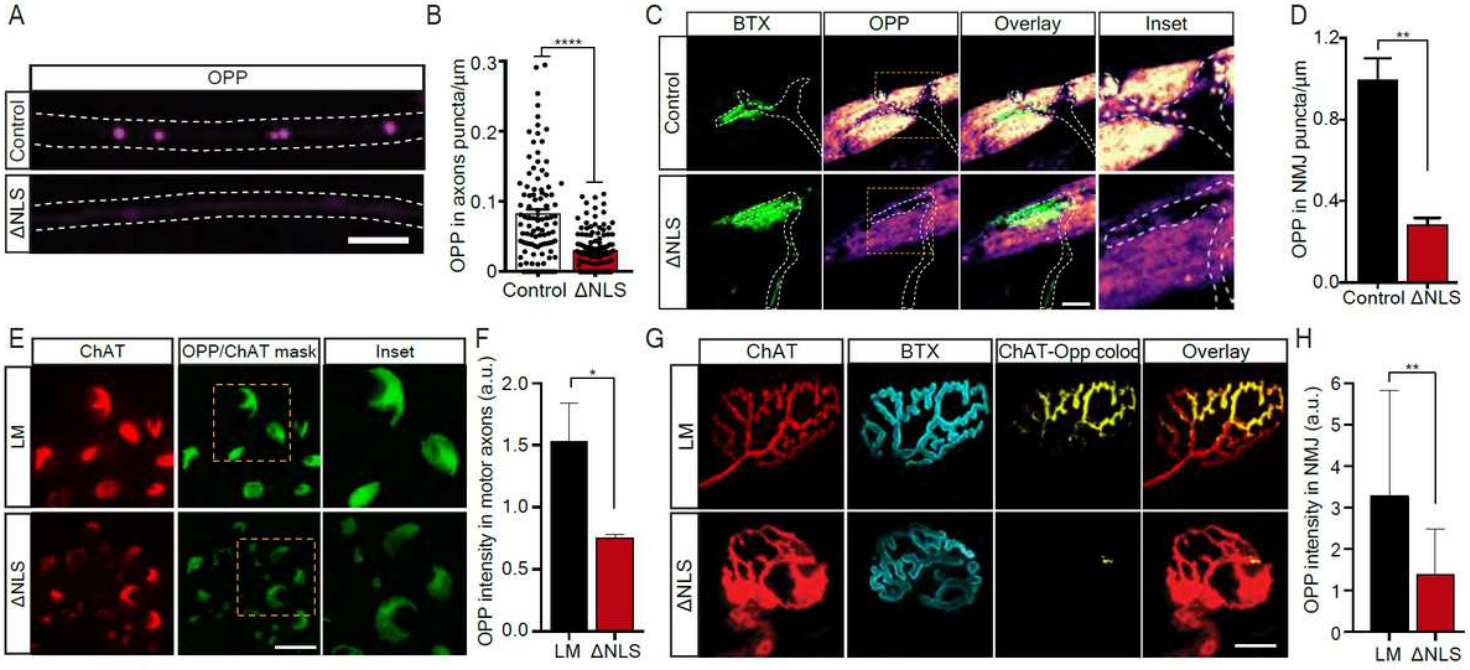

Figure 3

TDP-43 axonal accumulation leads to reduction of local protein synthesis in MN axons and NMJs. A) Representative images and B) quantification of OPP puncta density in distal MN from TDPΔNLS axons with (control) and without dox (ΔNLS). Scale bar = 5μm. n=100, 112 axons. Unpaired two-tail student's t-test ****p<0.0001. C) Representative images and D) quantification of OPP puncta density in in-vitro NMJs from TDPΔNLS MN axons with (control) and without dox (ΔNLS). Scale bar = 5μm. Data is shown as the mean ± SEM. n=3 average of 3 independent repeats, unpaired two-tail student's t-test **p<0.01. E) Representative images and F) quantification of OPP labeled SN sections shows OPP labeling in ChAT:RosatdTomato MN axons of TDPΔNLS mice compared to LM control mice. Scale bar = 10μm. Data is shown as the mean ± S.E. n=3 the averages of 3 independent repeats from 3 mice in each condition. *p<0.05 unpaired two-tail student's t-test. G) Representative images and H) quantification of pre-synaptic axons (ChAT:RosatdTomato) in TA muscle NMJs. Scale bar = 10μm. Data is shown as the mean ± SD. n=24, 19 NMJs from 3 mice of each condition. Unpaired two-tail student's t-test **p<0.01.

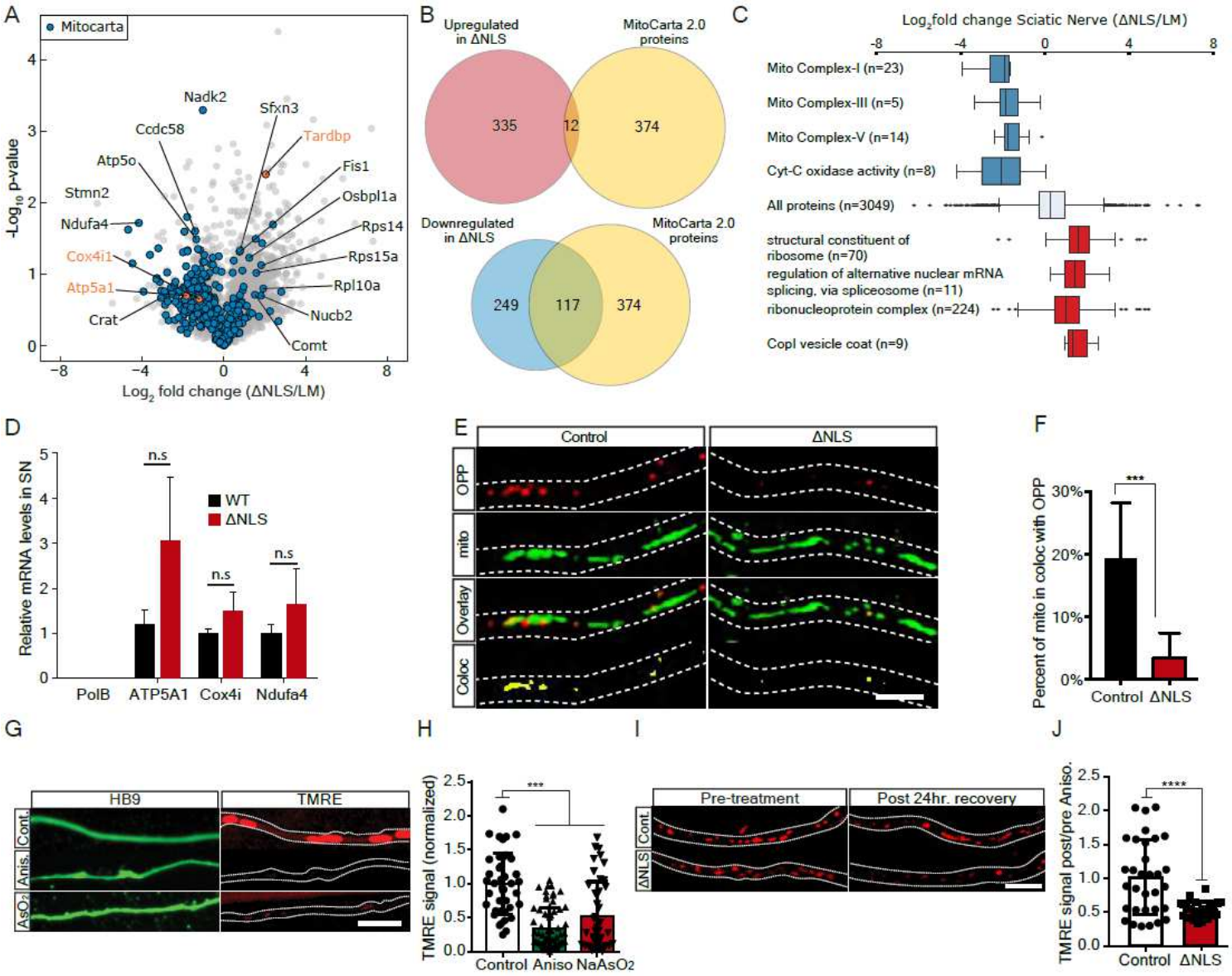

Figure 4

TDP-43 Axonal Accumulation Reduces Levels of Nuclear-Encoded Mitochondrial Proteins and Decreases Mitochondria-Associated local synthesis. A) Volcano plot representing SN proteome analysis of TDPΔNLS and LM mice. Data is shown as Log2FC of TDPΔNLS over LM proteome. n=4 sciatic nerve axoplasm preparations from each condition. Nuclear-encoded mitochondrial proteins marked in blue (Mitocarta). Cox4i1 and ATP5A1 (labeled orange) were chosen for further characterization. B) Venn diagram comparing all mitocarta proteins in our dataset with proteins that were up-regulated (upper panel) or down-regulated (lower panel). Log2FC>1 for up-regulated and <-1 for down-regulated proteins. C) GO analyses categories of proteome results. Blue indicates down-regulated proteins, red up-regulated. D) qRT-PCR of nuclear-encoded mitochondria protein mRNA levels in SN axoplasm from TDPΔNLS and LM mice. mRNA levels were normalized to total mitochondria content, as measured by mitochondria-encoded mRNA, RNR2. PolB mRNA was measured to identify no contamination of nuclear RNA. n=3, 3 SNs. One-way Anova with Holm-Sidak correction revealed no significant differences. E) Representative

images and F) quantification of OPP (red) and mitotracker (green) colocalization in distal axons. The percent of mitochondria in colocalization with OPP in distal axons in ΔNLS axons compared with control axons. Data is shown as the mean percent of mito-OPP colocalization ± SD. Scale bar = 5μm. n=43 (control), 36 (ΔNLS) axons from 3 independent repeats. Unpaired two-tail student's t-test ***p>0.001. G) Representative images and H) quantification of TMRE signal in control axons (n=40), in axons treated with protein synthesis inhibitor anisomycin (n=69) or treated with NaAsO2 (n=43). Scale bar =10μm. Data is shown as the mean TMRE signal. One-way ANOVA with Holm-Sidak correction ***p<0.001. I) Representative images J) and quantification of TMRE signal in ΔNLS and control MN axons cultured in MFC. Protein synthesis of distal axons was transiently inhibited for 4 hours and then washed out. Axons were left to recover for 24 hours, after which TMRE signal was collected from distal axons. Data is shown as the mean percent of TMRE signal post/pre protein synthesis inhibitors ± SD. n=32 ,29 axons. unpaired two-tail student's t-test ****p<0.0001.

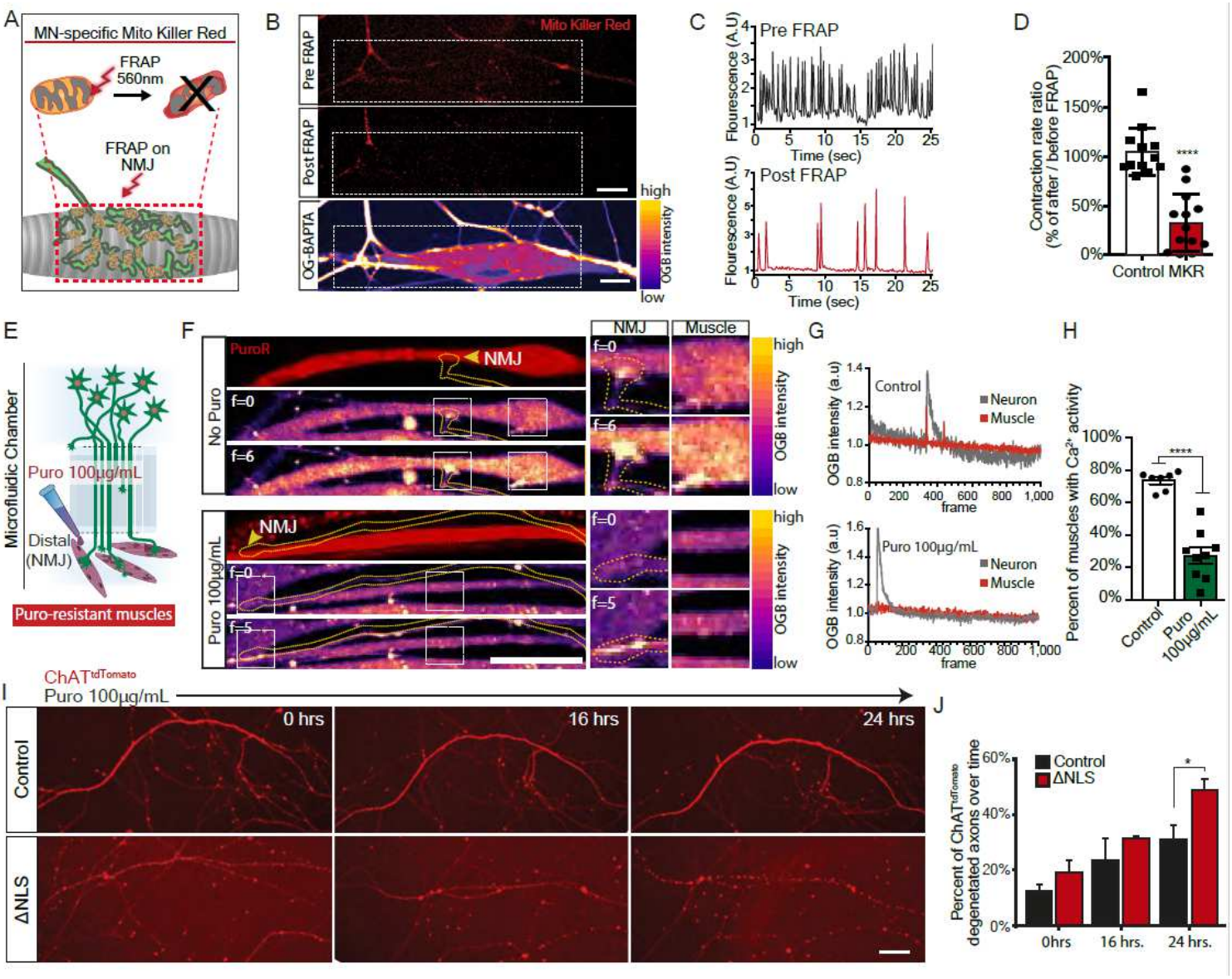

Figure 5

NMJ function is dependent on mitochondria and local synthesis, and their absence leads to decreased NMJ activity and axon degeneration. A) Schematic illustration of Mito-Killer-Red (MKR) experimental setup. MNs are cultured in MFCs and induced to express MKR using lentiviral infection. Myocytes are plated on the distal compartment of MFC. MKR is bleached at the NMJ with a 560nm laser leading to mitochondrial damage. B) Representative images of MKR (red) in pre-synaptic axons before, and after bleach (white dashed line indicates bleached region). Lower panel depicts a muscle and its innervating axon, all visualized by Oregon-Green BAPTA (OGB), which was also used for measuring the calcium transients in muscles before and after MKR activation. C-D) Time traces of the OGB intensity indicating muscle contraction (C) and quantification (D) of contraction ratio before and after MKR pre-synaptic bleaching (n=13). Bleaching pre-synaptic axons expressing ChAT:RosatdTomato and not MKR served as a control (n=12). Scale bar = 10μm. Data is shown as the mean ± S.D. unpaired two-tail student's t-test ****p<0.0001. E) Schematic illustration of experimental procedure. Healthy MNs were co-cultured with muscles that were pre-transfected with PQCXIP-mCherry empty vectors expressing puromycin-resistance gene (PAC). Upon NMJ maturation, Puromycin (100μg/mL) was added exclusively to the NMJ compartment for 16 hours before labeling of the co-cultures with OGB, and imaging. F) Left panel: Representative images from time series movies of calcium indicator OGB-labeled co-cultures. Right panel: The images demonstrate paired axon-muscle calcium activity only in control NMJs, but not in co-cultures treated distally with puromycin (100μg/mL), the pre-synaptic calcium release does not translate into efficient neurotransmission. Scale bar: 20μm. G) Representative time traces of calcium activity in pre-synaptic neurons and post-synaptic muscles show paired activity in control cultures (upper plot), and unpaired activity in puromycin-treated cultures (lower plot). H) Quantitative analysis of the percent of innervated and contracting muscles after inhibition of axonal and pre-synaptic local synthesis. n=7 (control) and 9 (puro) MFC co-cultures from 3 independent experiments, ****p<0.0001 unpaired two-tail student's t-test. I) Representative images and J) quantification of the percent of degenerating axons in the distal compartment of ΔNLS and control MN axons following 16 and 24h of puromycin treatment. Scale bar = 50μm. Data is shown as the mean percent of degenerating axons (length) per total axons (length) in MFC ± S.D. n = 4 (control) MFCs, and 3 (ΔNLS) MFCs, all from 3 independent repeats. One-way ANOVA with Holm-Sidak correction *p<0.05.

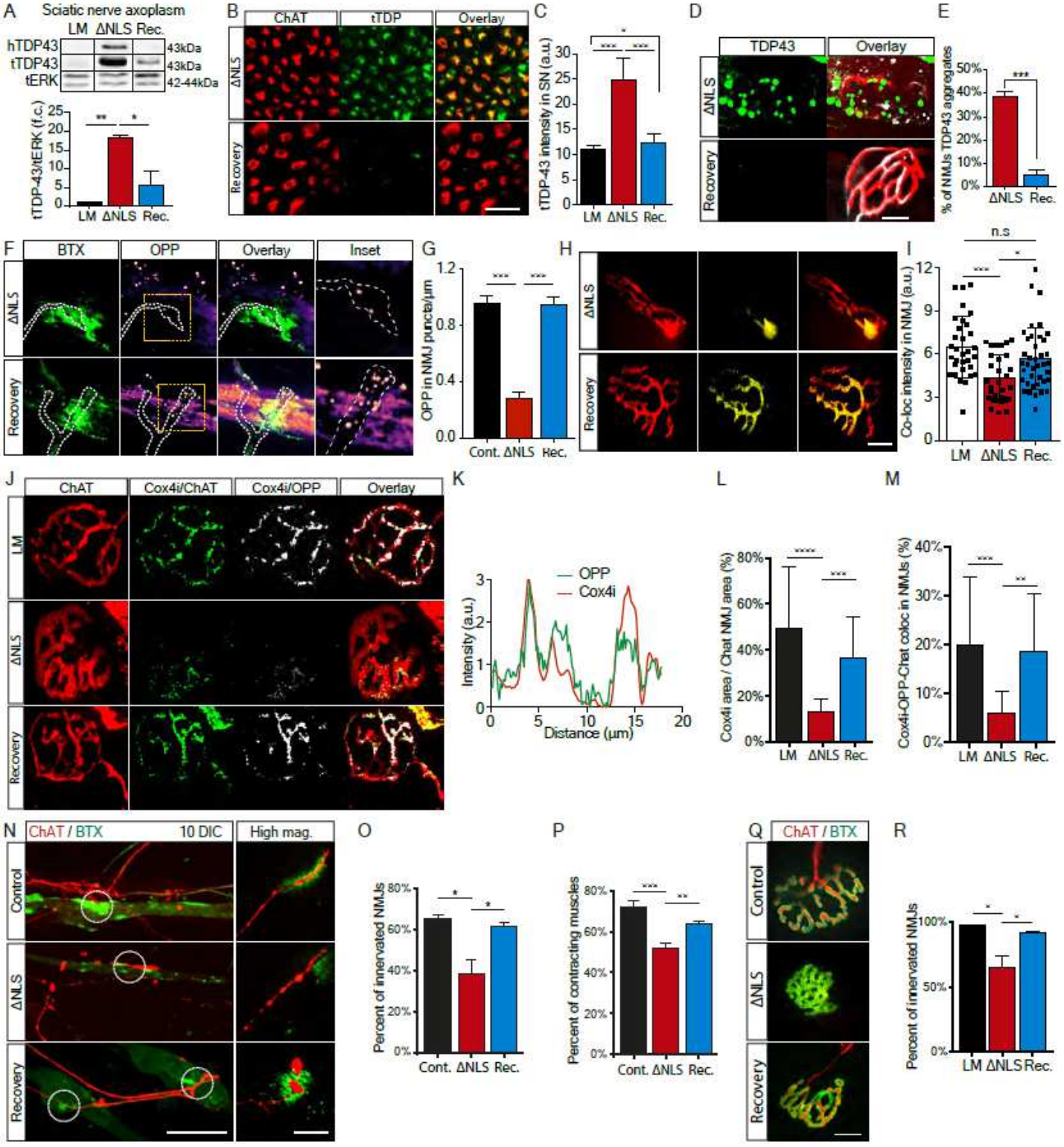

Figure 6

Restoring TDP-43 localization recovers local translation of mitochondrial proteins in distal axons and the NMJs, and enables functional reinnervation. A) Western-blot image (upper panel) and quantification (lower panel) of mice sciatic nerves (SNs) from LM, TDPΔNLS, and TDPΔNLS after dox re-application (recovery), blotted for total-TDP-43 (tTDP-43) and human-TDP-43 (hTDP-43). tERK used as a loading control. Signal calculated as the tTDP-43 signal normalized to the tERK signal. Data is shown as the

mean ± S.E. n=3 SN axoplasm preparations, one-way ANOVA with Holm-Sidak correction, *p<0.05, **p<0.01. B) Representative images and C) quantification of TDP-43 (green) immunolabeled ChATtdTomato-TDPΔNLS (Chat-red) SN sections from LM (control), ΔNLS, and Recovery (Rec.) mice. Scale bar = 20μm. Data is shown as the mean tTDP-43 intensity in SN ± S.D. n=34 (control), 34 (ΔNLS), 33 (rec) SN sections imaged from 3 mice in each condition. One-way ANOVA with Holm-Sidak correction *p<0.05, ***p<0.001. D) Representative images of NMJ labeling for TDP-43 (green) with postsynaptic BTX (red) and pre-synaptic NFH (grey), and E) quantification of the percent of NMJs with apparent TDP-43 aggregates. Scale bar = 10μm. Data is shown as the mean ± SE. n=3 mice from each condition. Unpaired two-tailed student's t-test ***p<0.001. F) Representative images and G) analysis of the OPP puncta density in NMJs from TDPΔNLS MNs without dox (ΔNLS) and with dox reintroduction (Recovery) and with constant dox application (Cont.). Scale bar = 5μm. Data is shown as the mean number of OPP puncta/μm ± S.E. n=3 average of 3 independent biological repeats, one-way ANOVA with Holm-Sidak correction, ***p<0.001. H) Representative images and I) analysis of the OPP labeling intensity in pre-synaptic compartment in NMJs of TA muscle from LM n=32 NMJs, ΔNLS n=30 NMJs, and recovery mice n=39,NMJs. All from 3 mice. Data is shown as the mean OPP-ChAT colocalization intensity ± S.D. Scale bar = 10μm. One-way ANOVA with Holm-Sidak correction, *p<0.05, ***p<0.001. J) Representative co-localization images of mitochondria protein Cox4i (green) with pre-synaptic ChAT (red) and OPP labeling (gray) in NMJs from LM, ΔNLS, and recovered mice. Scale bar = 10μm. K) Representative histogram of Cox4i (red) and OPP (green) signals within NMJ pre-synapse. L) Quantitative colocalization analysis of the percent of Cox4i area within the pre-synapse area (ChATtdTomato) in LM, ΔNLS, and recovered mice. Data is shown as the mean percent of Cox4i-ChAT colocalization ± S.D. n=21, 23, 13 NMJs. 3 mice from each group. One-way ANOVA with Holm-Sidak correction, ****p<0.0001, ***p<0.001. M) Quantitative analysis of Cox4i colocalization with OPP in the pre-synaptic NMJ (ChATtdTomato) from LM, ΔNLS, and recovered mice. Data is shown as the mean percent of Cox4i-OPP colocalization area ± S.D. n=21, 23, 13 NMJs from 3 mice of each group. One-way ANOVA with Holm-Sidak correction, ***p<0.001, **p<0.01. N) Representative images and O) quantification of in-vitro NMJ innervation by structural (measured as the percent of ChATtdTomato positive BTX clusters) and P) functional aspects (measured as the percent of innervated and contracting muscles from total innervated muscles). NMJ re-innervation was measured in control, ΔNLS and recovery co-cultures. Scale bar = 40μm in large image, 5μm in inset. Data is shown as the mean ± S.E. For I, n=3,3,3 MFCs for each condition. For K, n=7,6,7 MFCs. Both from 3 independent repeats. One-way ANOVA with Holm-Sidak correction, *p<0.05, **p<0.01, ***p<0.001. Q) Representative images of NMJs from LM, ΔNLS, and recovered mice. Scale bar = 10μm. R) Quantification of the percentage of innervated NMJs in ChATtdTomato-LM, TDPΔNLS and Recovery mice calculated as percent of NMJs with BTX (post-synaptic) colocalization with Chat signal (pre-synaptic). Data is shown as the mean ± S.E. n=3 mice from each condition. One-way ANOVA with Holm-Sidak correction *p<0.05

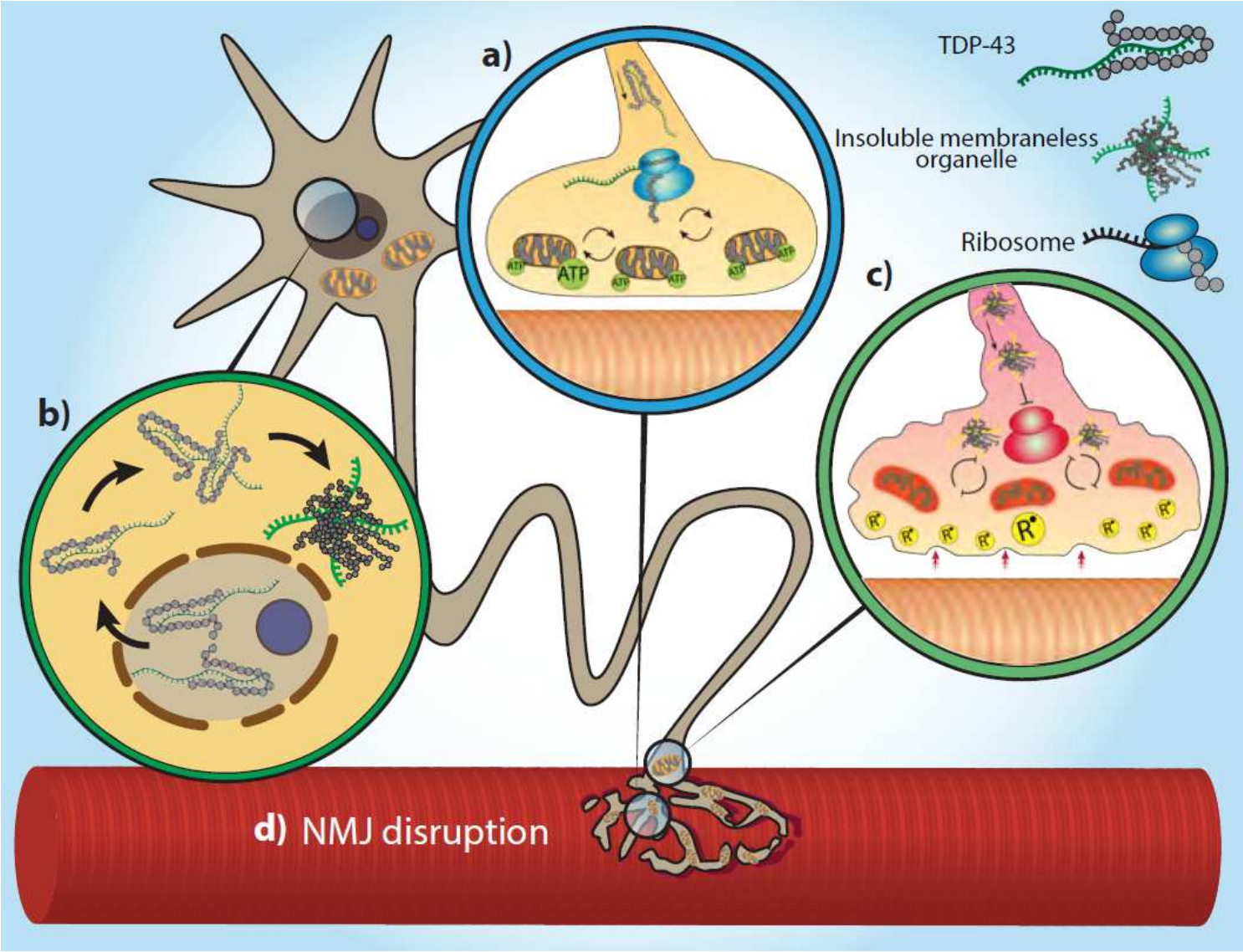

Figure 7

Model: TDP-43 axonal mislocalization creates RNPs which decrease local translation of nuclear-encoded mitochondrial proteins, leading to NMJ degeneration. a) TDP-43 is regularly found in axons and NMJs in controlled amounts and supports axonal and synaptic local translation by shuttling mRNAs. b-c) Cytoplasmic mislocalization of TDP-43 in ALS (b) promotes its axonal accumulation in RNP condensates that sequester mRNAs and interferes with local translation, especially of nuclear-encoded mitochondrial proteins (c). This process leads to synaptic mitochondria toxicity and eventually to NMJ dysfunction and degeneration (d).

Supplementary Files

This is a list of supplementary files associated with this preprint. Click to download.

- AltmanIonescuSupMovie1.mov

- AltmanIonescuSupMovie2.mov
- AltmanIonescuSupMovie3.mov
- AltmanIonescuSupMovie4.mov
- AltmanIonescuSupMovie5.mov
- AltmanIonescuSupMovie6.mov
- SupFiguresa.pdf
- Supplementaryfigurelegends.pdf
- TDP43Experiment01ReanalysisCanonicalFASTA.xlsx